A MASTER'S THESIS

A NUMERICAL ANALYSIS OF THE WAVE FORCES ON VERTICAL CYLINDERS BY BOUNDARY ELEMENT METHOD

CHEJU NATIONAL UNIVERSITY GRADUATE SCHOOL

Department of Civil & Ocean Engineering

Cao Tan Ngoc Than

February 2009

A NUMERICAL ANALYSIS OF THE WAVE FORCES ON VERTICAL CYLINDERS BY BOUNDARY ELEMENT METHOD

Cao Tan Ngoc Than

(Supervised by Professor Nam-Hyeong Kim)

A thesis submitted in partial fulfillment of the requirement for the Degree of Master of Engineering

2009.2

This thesis has been examined and approved

Thesis director, Sang-Jin Kim, Prof. of Civil & Ocean Engineering

Thesis director, Byoung-Gul Lee, Prof. of Civil & Ocean Engineering

Thesis director, Nam-Hyeong Kim, Prof. of Civil & Ocean Engineering

February.2009

Department of Civil & Ocean Engineering

GRADUATE SCHOOL

CHEJU NATIONAL UNIVERSITY

CONTENTS

List of Figures

Summary

With the advances in the design and construction, various types of offshore structures are now commonly constructed with a composite configuration of several legs such as cylinders. Thus, the interaction between waves and multiple cylinders is becoming more and more important. The wave pressure and wave forces acting on the cylinders must be exactly estimate to evaluate the wave effects and the stability of structures.

The interaction between waves and offshore structures causes problems such as diffracted waves, reflected waves, and wave forces. Consider N large vertical circular cylinders placed on the bottom. As the incident waves impinge on each cylinder, the reflected waves move outward. On the sheltered side of the cylinders there will be a “shadow” zone where the wave fronts are bent around the cylinders, the so-called diffracted waves. The reflected waves and diffracted waves, combined, are usually called the scattered waves. The scattered waves of each cylinder can affect other cylinders in the group. This process is generally termed diffraction. By the process of diffraction the pressure around the cylinders will be changed and therefore the forces on the cylinders will be influenced. The problems could be dealt with the boundary value with the velocity potential.

There have been several studies dealing with the interaction of water waves and multiple cylinders. Twersky (1952) constructed a solution using an iterative procedure in which successive scattered waves by each of the cylinders were introduced at each other. This method was extended to the water wave case by Ohkusu (1974). The main drawback of the iterative procedure is that it rapidly becomes unmanageable as the number of the cylinders increases. Another approach is the direct matrix method, Spring and Monkmeyer (1974) proposed a solution for the interaction of water waves and the cylinders using eigenfunction expansion approach. They formulated the problem in terms of matrix equation and the solution is obtained by the inversion of the matrix.

Chakrabarti (1978) extended the work of Spring and Monkmeyer (1974), and obtained the solution for the diffracted wave of multiple cylinders by carrying out the analysis in a complex domain. Subsequently, Linton and Evan (1990) made a major simplification to the theory proposed by Spring and Monkmeyer (1974).

On the other hand, there are many studies to solve the diffraction problems of water waves by using boundary element method. Notably, Kim and Park (2007) studied a numerical analysis method to calculate the wave force on isolated vertical circular cylinder by boundary element method and the numerical results of their study are strong agreement with those of MacCamy and Fuchs (1954). Also, Kim and Cao (2008) studied wave forces acting on the two vertical cylinders and three vertical cylinders in water waves.

The boundary element method is divided into direct boundary element method and indirect boundary element method. The direct boundary element method derives from the integral equation by Green's or Cauchy's theory. This deriving process is solved by the special application of weighted residual method and it has general integral formulation. Derived integral equation is divided into two parts: the unknown functions and the derivatives of normal direction. One side of them generally has unknown values. The indirect boundary element method is derived integral equation in boundary conditions and is made operation function by singular value of governing equation. The coefficient that is involved operation function is unknown value in direct boundary element.

In this paper, a numerical analysis by boundary element method for calculating wave forces acting on multiple cylinders is presented. The numerical analysis method by Green function in direct boundary element method using velocity potential ϕ is developed. Attention has been concentrated on wave forces on N large vertical cylinders, having radius a and placed on the bottom. To verify this numerical method and to investigate the effect of the neighboring cylinders on the wave forces acting on a cylinder, two-cylinder configuration and three-cylinder configuration are used in this study. The wave forces acting on two vertical circular cylinders and three vertical

cylinders obtained from this numerical method are compared with those of Ohkusu (1974) and Chakrabarti (1978). The comparisons show that the computed results of this study are strong agreement with their results. Also in this study, several numerical examples are given to illustrate the effects of various parameters on the wave forces acting on the cylinders such as the cylinder spacing, the wave number, and the incident wave angle. The run-up and free surface elevation around two vertical cylinders and three vertical cylinders are also calculated.

Chapter 1
INTRODUCTION

1.1 Background

Recently with the advances in the design and construction, various types of offshore structures are now commonly constructed with a composite configuration of several legs such as cylinders. Thus, the interaction between waves and group of cylinders is becoming more and more important. The wave pressure and wave forces acting on the cylinders must be exactly estimate to evaluate the wave effects and the stability of structures.

The interaction between waves and offshore structures causes problems such as diffracted waves, reflected waves, and wave forces. Consider N large vertical cylinders placed on the bottom. As the incident waves impinge on each cylinder, the reflected waves move outward. On the sheltered side of the cylinders there will be a “shadow” zone where the wave fronts are bent around the cylinders, the so-called diffracted waves. The reflected waves and diffracted waves, combined, are usually called the scattered waves. The scattered waves of each cylinder in the group cylinders can affect other cylinders. This process is generally termed diffraction. By the process of diffraction the pressure around the cylinders will be change and therefore the forces on the cylinders will be influenced. The problems could be dealt with the boundary value with the velocity potential.

Linear diffracted wave theory which uses linear free surface conditions proposes many different methods because the linear diffracted wave theory is easy and simple. The diffracted wave problem of a vertical cylinder was initially developed by Havelock (1940) for the special case of infinite water depth. MacCamy and Fuchs (1954) proposed a linear theory for the problem of diffraction of plane waves from a vertical circular cylinder in the case of finite water depth and the results are exact to the first order.

After these researches, there have been many studies dealing with the interaction of waves and multiple cylinders. Twersky (1952) constructed a solution using an iterative procedure in which successive scattered waves by each of the cylinders were introduced at each other. This method was extended to the water wave case by Ohkusu (1974). The main drawback of the iterative procedure is that it rapidly becomes unmanageable as the number of the cylinders increases. Another approach is the direct matrix method, Spring and Monkmeyer(1974) proposed a solution for the interaction of water waves and the cylinders using eigenfunction expansion approach. They formulated the problem in terms of matrix equation and the solution is obtained by the inversion of the matrix. Chakrabarti (1978) extended the work of Spring and Monkmeyer, and obtained the solution for the diffracted wave of multiple cylinders by carrying out the analysis in a complex domain. Subsequently, Linton and Evan (1990) made a major simplification to the theory proposed by Spring and Monkmeyer.

1.2 Objectives

In recent years, the Boundary Element Method has emerged as a strong numerical method for investigating dynamic problems especially for radiation and scattering problems. The reasons are that the boundary integral equation satisfies radiation condition automatically and correctly, and for linear problems only the surface of the boundaries need to be discrestized.

The boundary element method is divided into direct boundary element method and indirect boundary element method. The direct boundary element method derives from the integral equation by Green's or Cauchy's theory. This deriving process is solved by the special application of weighted residual method and it has general integral formulation. Derived integral equation is divided into two parts: the unknown functions and the derivatives of normal direction. One side of them generally has unknown values. The indirect boundary element method is derived integral equation in boundary conditions and is made operation function by singular value of governing equation. The coefficient that is involved operation function is unknown value in direct boundary element.

Basing on boundary element method, there are many studies to solve the diffraction problems of water waves and structures. Notably, Kim and Park (2007) studied a numerical analysis method to calculate the wave forces on isolated vertical circular cylinder by boundary element method and their numerical results are strong agreement with those of MacCamy and Fuchs (1954). Also, Kim and Cao (2008) studied wave forces acting on two vertical cylinders and three vertical cylinders in water waves.

The main objectives of this study are to solve the diffraction problem of water waves by multiple cylinders by using boundary element method. In this study, a numerical analysis by boundary element method using velocity potential ϕ is developed. Once the wave velocity potential is known, the wave pressure, wave forces acting on the cylinders can be calculated by using it. Also, the wave run-up on the outer walls of the cylinders and free-surface elevation around the cylinders are calculated in this study.

1.3 Study Contents

A numerical analysis by boundary element method for calculating wave forces acting on multiple cylinders is described in this study. The numerical analysis method by Green function in direct boundary element method using velocity potential ϕ is developed. To verify this numerical analysis and to investigate the effect of the neighboring cylinders on the wave forces on a cylinder in the group, two-cylinder configuration and three-cylinder configuration are used in this study. The numerical results are carried out as follows:

(1) The wave forces acting on two cylinders and three cylinders are computed.

(2) To verify this method, the numerical results obtained from this study are compared with those of Ohkusu (1974) and those of Chakrabarti (1978).

(3) The effects of the cylinder spacing and wave angular frequency on the wave forces acting on the cylinders are analyzed.

(4) Also, the effects of incident wave angle on wave forces are investigated in this study.

(5) The run-up on outer walls of the cylinders and the free-surface elevation around the cylinders are also calculated.

Chapter 2
FORMULATION OF BOUNDARY ELEMENT ANALYSIS

2.1 Diffraction Phenomenon

This section will describe the diffraction phenomenon of waves by multiple vertical cylinders. Attention has been concentrated on the interaction of N vertical cylinders with the incident waves where the cylinder diameter D is assumed to be much larger than the wave length L. As the incident waves impinge on each cylinder, the reflected waves move outward. On the sheltered side of the cylinders there will be a "shadow" zone where the wave fronts are bent around the cylinders, the so-called diffracted wave. The reflected waves and diffracted waves, combined, are usually called the scattered waves. The scattered waves of each cylinder can affect the other cylinders in the group. This process is generally termed diffraction. By the process of diffraction the pressure around the cylinders will be changed and therefore the forces on the cylinders will be influenced. It is generally accepted that the diffraction effect becomes important when the ratio D/L becomes larger than 0.2 (Issacson, 1979).

Normally, in the diffraction flow regime, the flow around the circular cylindrical bodies is unseparated. This can be shown by the following analysis:

The amplitude of the horizontal component of water-particle motion at the sea surface is as follows:

$$a = \frac{H}{2} \times \frac{1}{\tanh(kh)} \tag{1}$$

where H is the wave height, h is the water depth and k is the wave number.

$$k = \frac{2\pi}{L} \tag{2}$$

The Keulegan-Carpenter number for a vertical circular cylinder will then be:

$$KC = \frac{2\pi a}{D} = \frac{\pi (H/L)}{(D/L)\tanh(kh)} \tag{3}$$

The largest KC number is obtained when the maximum wave steepness is reached, namely when $H/L = (H/L)_{\max}$. The latter may be given approximately as (Isaacson, 1979):

$$(\frac{H}{L})_{\max} = 0.14\tanh(kh) \tag{4}$$

Therefore, the largest KC number that the body would experience may be written as:

$$KC = \frac{0.44}{D/L} \tag{5}$$

If KC number is larger than this limiting value, the waves will break. Eq. (5) is plotted as a dashed line in Fig. 1. The vertical line $D/L = 0.2$ in Fig. 1 represents the boundary beyond which the diffraction effect becomes significant. Also, Fig. 1 indicates that the KC numbers experienced in the diffraction flow regime are extremely small, namely $KC < 2$. Fig. 2 shows that for $KC < 2$ the flow will be unseparated in most of the case.

The preceding analysis suggests that the problems regarding the flow around and forces on a large body in the diffraction regime may be analyzed by potential theory in most of the situations, since the flow is unseparated.

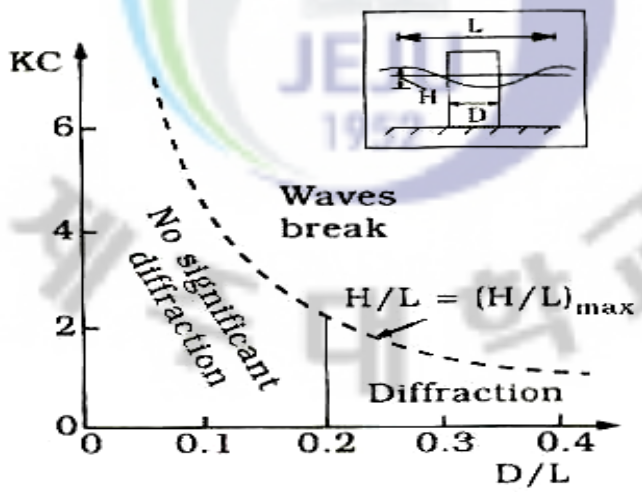

Fig. 1 Different flow regimes in the ($KC, D/L$) plane. Adapted from Isaacson (1979)

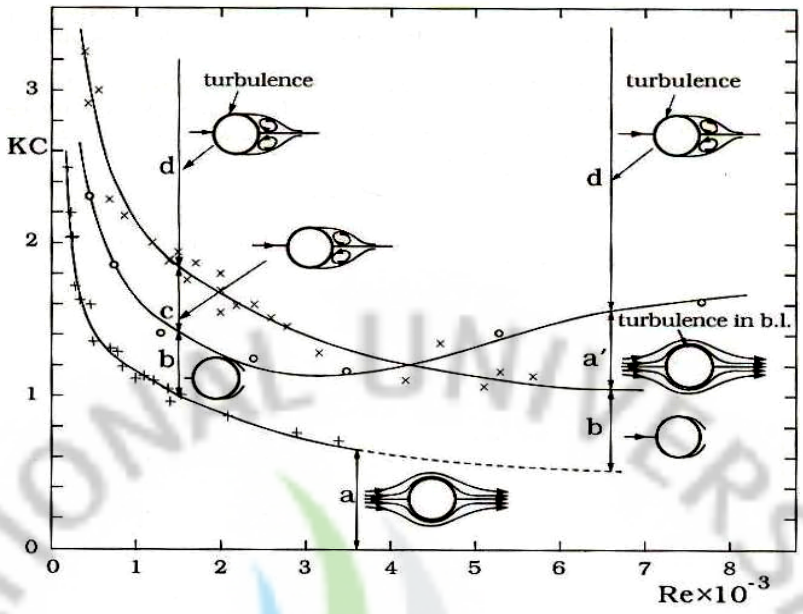

Fig. 2 Regimes of flow around a smooth, circular cylinder in oscillatory flow for small KC numbers ($KC < 3$). Data: Circles from Sarpkaya (1986a); crosses for $\mathrm{Re} < 1000$ from Honji (1981) and crosses for $\mathrm{Re} > 1000$ from Sarpkaya (1986a)

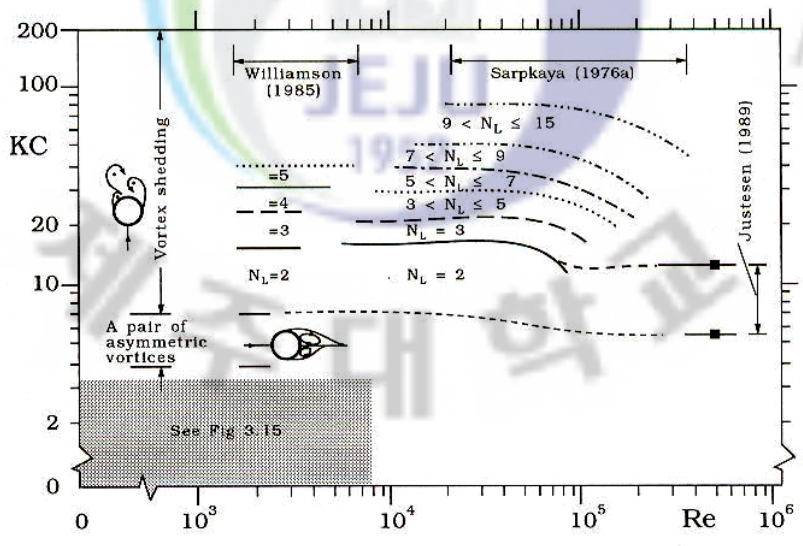

Fig. 3 Vortex-shedding regimes around a smooth circular cylinder in oscillatory flow. Data: Lines, Sarpkaya (1986a) and Williamson (1985) and: squares from Justesen (1989)

2.2 Basic Equations and Boundary Conditions

Considering N vertical circular cylinders, having radius a, are placed in the water of uniform depth h. The global Cartesian coordinate system (x, y, z) is defined with the origin located on the still-water level, the z axis directed vertically, x and y axis directed horizontally. The geometry of this problem is shown in Fig. 4.

As usual, it is assumed that the fluid is inviscid, incompressible, its motion is irritation. The cylinders subjected to a strain of regular wave of height H and angular frequency σ propagating at an angle β to the positive x axis.

The velocity potential $\Phi(x, y, z; t)$ can be defined by:

$$\Phi(x, y, z; t) = R_e[\phi(x, y, z)e^{-i\sigma t}] \tag{6}$$

where $R_e[]$ denotes the real part of a complex expression.

From the linear feature of potential flow, the total potential ϕ can be written as the sum of incident wave velocity potential and scattered wave velocity potential:

$$\phi = \phi_i + \phi_s \tag{7}$$

where ϕ_i is the velocity potential of incident wave and ϕ_s is velocity potential of the scattered wave.

The incident wave velocity potential ϕ_i is given as follows:

$$\phi_i = -i\frac{g}{\sigma}\frac{H}{2}\frac{\cosh k(h+z)}{\cosh kh}e^{ik(x\cos\beta + y\sin\beta)} \tag{8}$$

where $H/2$ is wave amplitude, g is the acceleration due to gravity, i is the imaginary unit $i = \sqrt{-1}$, k is the wave number ($k = 2\pi / L$; L: wave length). The quantity σ is the angular frequency and related to wave number k by the dispersion relation:

$$\sigma^2 = gk\tanh(kh) \tag{9}$$

It is known that the incident wave potential function in Eq. (8) satisfies boundary conditions.

Boundary problems by the formulation of scattered wave velocity potential ϕ_s are given as follows:

- Laplace equation:

$$\nabla^2 \phi_s = 0 \qquad (\text{in } \Omega) \qquad (10.a)$$

- Free surface boundary condition:

$$\frac{\partial \phi_s}{\partial z} - \frac{\sigma^2}{g}\phi_s = 0 \qquad (\text{on } \Gamma_F) \qquad (10.b)$$

- Cylinder surface boundary condition:

$$\frac{\partial \phi_s}{\partial n} = -\frac{\partial \phi_i}{\partial n} \qquad (\text{on } \Gamma_{H_m}, m = 1,..., N) \qquad (10.c)$$

- Sea bed boundary condition:

$$\frac{\partial \phi_s}{\partial z} = 0 \qquad (\text{on } \Gamma_B) \qquad (10.d)$$

- Radiation boundary condition:

$$\lim_{R\to\infty} \sqrt{R}\{\frac{\partial \phi_s}{\partial R} - ik\phi_s\} = 0 \qquad (\text{on } \Gamma_R) \qquad (10.e)$$

where Ω is the fluid region, Γ_F is the free surface, $\Gamma_{H_m}, m = 1,..., N$ is the body surfaces of N cylinders, Γ_B is the sea bed, Γ_R is the virtual boundary at infinity, n is the outward unit normal on the boundary, and $R = \sqrt{x^2 + y^2}$.

The incident wave velocity potential can be defined as follows:

$$\phi_i = -i\frac{g}{\sigma}\frac{H}{2}\frac{\cosh k(h+z)}{\cosh kh}\Psi_i, \quad \Psi_i = e^{ik(x\cos\beta + y\sin\beta)} \qquad (11)$$

The scattered velocity potential is defined as follows:

$$\phi_s = -i\frac{g}{\sigma}\frac{H}{2}\frac{\cosh k(h+z)}{\cosh kh}\Psi_s(x, y) \qquad (12)$$

If the definitions of equations (11), (12) are substituted into Eqs.(10.a)~(10.e), the boundary value problems with Ψ_s are obtained as follows:

$$\nabla^2 \Psi_s + k^2 \Psi_s = 0 \qquad (\text{in } \Omega) \qquad (13.a)$$

$$\frac{\partial \Psi_s}{\partial n} = -\frac{\partial \Psi_i}{\partial n} \qquad (\text{on } S_{H_m}, m = 1,..., N) \qquad (13.b)$$

$$\lim_{R\to\infty} \sqrt{R}\{\frac{\partial \Psi_s}{\partial R} - ik\Psi_s\} = 0 \qquad (\text{on } S_\infty) \qquad (13.c)$$

In Eqs. (13.a)~(13.c), boundary value problems are two-dimension problems of $x-y$ plane as shown in Fig. 5. Finally, because of analyzing boundary value problems by Ψ_s, the scattered wave velocity potential is calculated. Then the total velocity potential, wave pressure, and wave forces are calculated by using it.

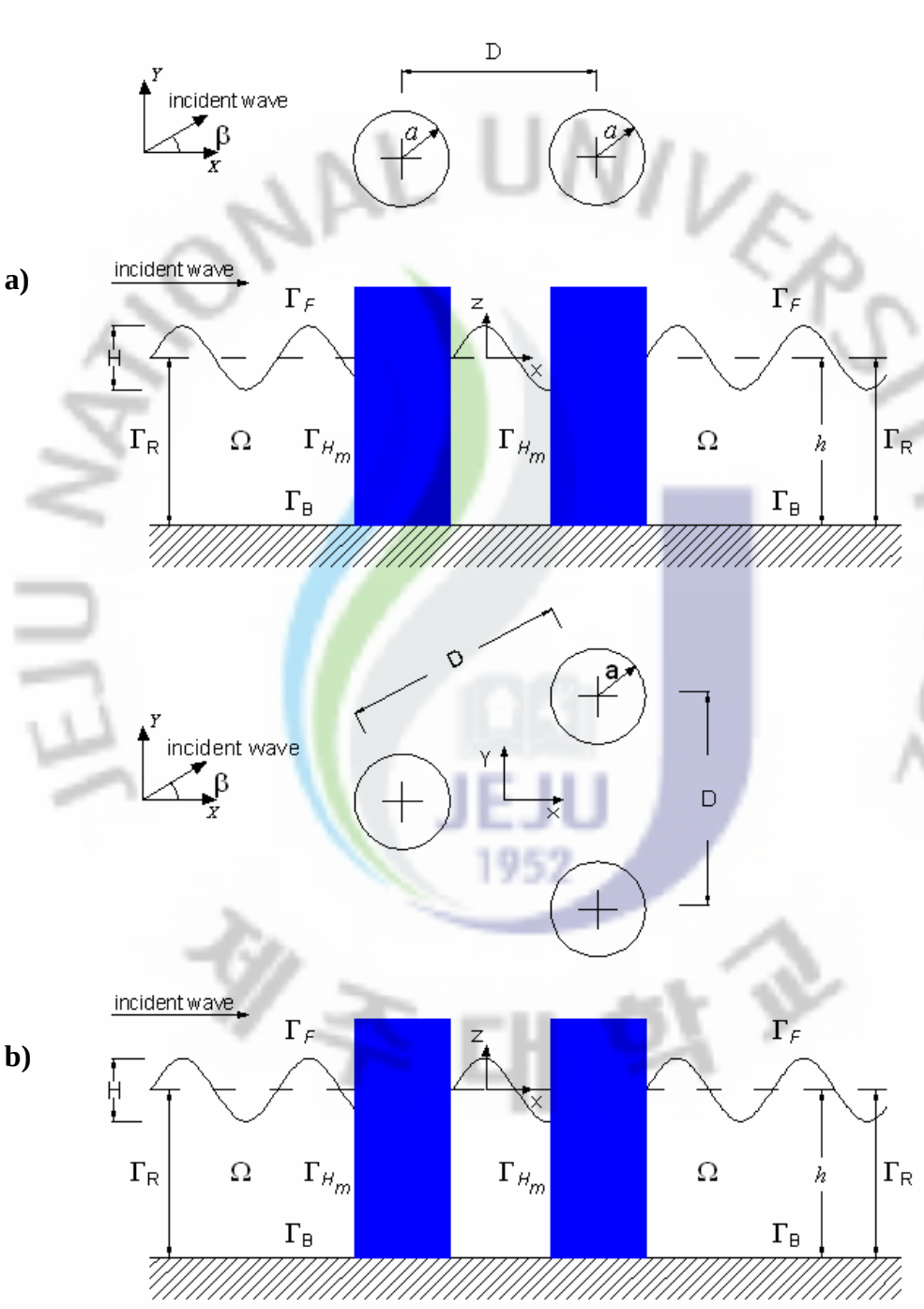

Fig. 4 Definition of: a) Two vertical circular cylinders,
b) Three vertical circular cylinders

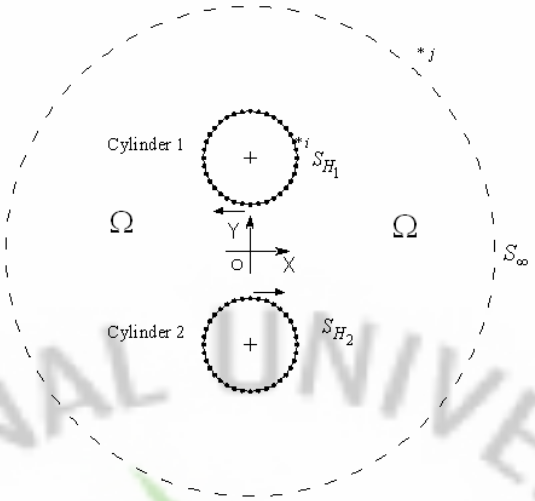

a) Two vertical circular cylinders

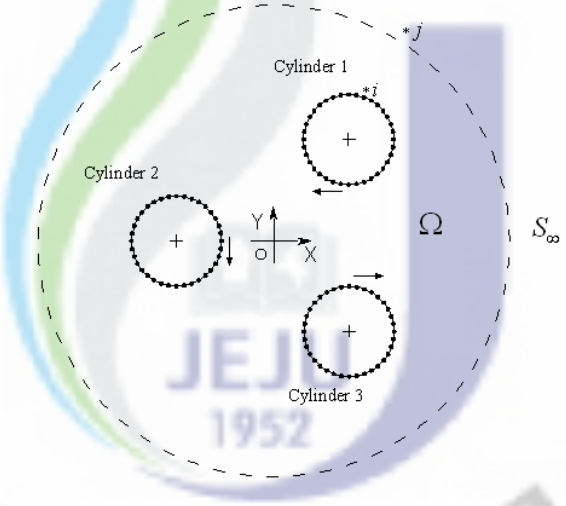

b) Three vertical circular cylinders

Fig. 5 Numerical model configurations:
a) Two vertical circular cylinders, b) Three vertical circular cylinders

2.3 Green Function

Green function plays an important role in the solution of partial differential equations, and is the key component to the development of boundary element method. Green function is a two-point function and it has peculiarity of $1/r$, excludes special point in case $r=0$. Green function satisfies the Laplace equation and other boundary conditions except the boundary condition at the body surfaces.

$$\nabla^2 G = -\delta(x-\xi)\delta(y-\eta)\delta(z-\zeta) \qquad (\text{in } \Omega) \qquad (14)$$

$$\frac{\partial G}{\partial z} - \frac{\sigma^2}{g} G = 0 \qquad (\text{on } \Gamma_F) \qquad (15)$$

$$\frac{\partial G}{\partial z} = 0 \qquad (\text{on } \Gamma_B) \qquad (16)$$

$$\lim_{r\to\infty} \sqrt{r}\{\frac{\partial G}{\partial r} - ik_0 G\} = 0 \qquad (\text{on } \Gamma_R) \qquad (17)$$

where G is Green function, δ is Dirac Delta function and (ξ,η,ζ) is the coordinate of the point in the fluid region.

According to John (1950), the Green function is derived as follows:

$$G(P,Q) = i\frac{(k_0^2-\nu^2)\cosh k_0(h+\zeta)}{2\{h(k_0^2-\nu^2)+\nu\}}\cosh hk_0(h+z)H_0^{(1)}(k_0 r)$$

$$+\sum_{n=1}^{\infty}\frac{(k_n^2+\nu^2)\cos k_n(h+\zeta)}{\pi\{k_n(k_n+\nu^2)-\nu\}}\cosh k_n(h+z)K_0(k_n r) \qquad (18)$$

$$r = \sqrt{(x-\xi)^2+(y-\eta)^2}$$

where, $H_m^{(1)}$: denotes the Hankel function of the first kind order m; K_m: denotes the modified Bessel function of the second kind order m; k_n $(n=0,1....)$: are the roots of the dispersion relation for free surface ($k_n \tan(k_n h) = -\sigma^2/g$) and are increasing size $(k_1 < k_2 < ...)$. Also, $\nu = \sigma^2/g$; $P(\xi,\eta,\zeta)$ and $Q(x,y,z)$ are two points in the fluid region.

2.4 Derivation of Integral Equations

The basic step in boundary element method is transforming the governing differential equation into an integral equation. The governing Laplace's equation for scattered wave potential ϕ_s (Eq. (10.a)) can be transformed into an integral equation by using the method of weighted residual:

$$\int\int\int_{\Omega} \nabla^2\phi_s G d\Omega = 0 \tag{19}$$

where the test function G is Green function.

The integral equation of scattered wave potential in the domain Ω (Eq. 19) can be transformed into boundary integral equation on the boundary S via Green's second identity and the result as follows:

$$\int\int\int_{\Omega} (\phi_s \nabla^2 G - G\nabla^2\phi_s) d\Omega = \int\int_{S} (\phi_s \frac{\partial G}{\partial n} - G\frac{\partial \phi_s}{\partial n}) ds \tag{20}$$

where S is the boundary of the fluid domain Ω, n is the outward unit normal on the boundary. As shown in Fig. 4, the boundaries of the fluid domain are the cylinder surface boundaries $\Gamma_{H_m}, m = 1,..., N$, free-surface boundary Γ_F, sea bed boundary Γ_B, and the virtual boundary Γ_R. Thus Eq. (20) can be written as follows:

$$\int\int\int_{\Omega} (\phi_s \nabla^2 G - G\nabla^2\phi_s) d\Omega = \int\int_{\sum_{m=1}^{N}\Gamma_{H_m}} (\phi_s \frac{\partial G}{\partial n} - G\frac{\partial \phi_s}{\partial n}) ds + \int\int_{\Gamma_F} (\phi_s \frac{\partial G}{\partial z} - G\frac{\partial \phi_s}{\partial z}) ds$$
$$+ \int\int_{\Gamma_B} (\phi_s \frac{\partial G}{\partial z} - G\frac{\partial \phi_s}{\partial z}) ds + \lim_{R\to\infty} \int\int_{\Gamma_R} (\phi_s \frac{\partial G}{\partial R} - G\frac{\partial \phi_s}{\partial R}) ds \tag{21}$$

Due to scattered wave potential ϕ_s and Green function G satisfy the boundary conditions at Γ_F, Γ_B and Γ_R, the integral equations at the boundaries Γ_F, Γ_B and Γ_R on the right hand side of Eq. (21) are vanish. Therefore, Eq. (21) can be rewritten as follows:

$$\int\int\int_{\Omega} (\phi_s \nabla^2 G - G\nabla^2\phi_s) d\Omega = \int\int_{\sum_{m=1}^{N}\Gamma_{H_m}} (\phi_s \frac{\partial G}{\partial n} - G\frac{\partial \phi_s}{\partial n}) ds \tag{22}$$

Now employing the sifting property of the Dirac distribution, this yields:

$$\int\int\int_{\Omega} \phi_s \nabla^2 G d\Omega = -\gamma \phi_s(P) \tag{23}$$

Finally substituting Eq. (19) and Eq. (23) into Eq. (22), the integral equation is obtained as follows:

$$\gamma\phi_s(P) = -\int\int_{\sum_{m=1}^{N}\Gamma_{H_m}} (\phi_s \frac{\partial G}{\partial n} - G\frac{\partial \phi_s}{\partial n})ds \tag{24}$$

where, $\gamma = 1$ as the point P places in the domain Ω, and $\gamma = 1/2$ as the point P places on the boundary of the domain.

In two-dimensional problems (Fig. 5), if the observation point i is presented over the boundary S plane, the boundary value problems of Eqs. (13.a)~(13.c) with using Ψ_i, Ψ_s are defined by the integral equation as shown in Eq. (25):

$$\frac{1}{2}\Psi_{si} = -\int_{\sum_{m=1}^{N} S_{H_m}+S_\infty} (\Psi_s \frac{\partial G}{\partial n} - G\frac{\partial \Psi_s}{\partial n})ds \tag{25}$$

and rearranging, the results is derived as follows:

$$\frac{1}{2}\Psi_{si} + \int_{\sum_{m=1}^{N} S_{H_m}+S_\infty} \Psi_s \frac{\partial G}{\partial n} ds = \int_{\sum_{m=1}^{N} S_{H_m}+S_\infty} G\frac{\partial \Psi_s}{\partial n} ds \tag{26}$$

If observation point i is near S_{H_m}, the Eq. (26) is the integral equation for S_∞. When S_∞ is near S_{H_m} with $r >> 1$, $kr \cong r$, $r \cong R$, the Hankel function is given as follows:

$$\left.\begin{aligned} H_0^{(1)}(kr) &\cong \sqrt{\frac{2}{\pi kR}} e^{\left\{i(kR-\frac{\pi}{4})\right\}} \\ \frac{\partial H_0^{(1)}}{\partial R} &\cong ik\sqrt{\frac{2}{\pi kR}} e^{\left\{i(kR-\frac{\pi}{4})\right\}} \end{aligned}\right\} \quad (\text{on } S_\infty) \tag{27}$$

The integral term for S_∞ of Eq. (26) is substituted as follows:

$$\begin{aligned} &\int_{S_\infty} \Psi_s \frac{\partial G}{\partial R} ds - \int_{S_\infty} \frac{\partial \Psi_s}{\partial R} G ds \\ &= -\frac{1}{4i}\sqrt{\frac{2}{\pi k}} e^{-i\frac{\pi}{4}} \int_{S_\infty} \frac{e^{ikR}}{\sqrt{R}} \left(\frac{\partial \Psi_s}{\partial R} - ik\Psi_s \right) ds \\ &= -\frac{1}{4i}\sqrt{\frac{2}{\pi k}} e^{-i\frac{\pi}{4}} \int_0^{2\pi} e^{ikR} \sqrt{R} \left(\frac{\partial \Psi_s}{\partial R} - ik\Psi_s \right) ds \end{aligned} \tag{28}$$

By substituting Eq. (28) into Eq. (13.c), the result is obtained as follows:

$$\int_{S_\infty} \Psi_s \frac{\partial G}{\partial R} ds - \int_{S_\infty} \frac{\partial \Psi_s}{\partial R} G ds = 0 \tag{29}$$

Therefore, the finally boundary integral equation on scattered wave potential is given as follows:

$$\frac{1}{2}\Psi_{si} + \int_{\sum_{m=1}^{N} S_{H_m}} \Psi_s \frac{\partial G}{\partial n} ds = \int_{\sum_{m=1}^{N} S_{H_m}} G \frac{\partial \Psi_s}{\partial n} ds \tag{30}$$

Eq. (30) is the integral equation for the near curve $S_{H_m}, m = 1,..., N$ of the cylinder surfaces and the scattered wave velocity potential on the boundary is derived by solving this equation.

The scattered wave potential in the domain Ω can be calculated after the scattered wave potential on the boundary has been known. If the observation point i is placed in the domain Ω, the integral equation for scattered wave potential is given as follows:

$$\Psi_{si} = \int_{\sum_{m=1}^{N} S_{H_m}} \frac{\partial \Psi_s^e}{\partial n} G ds - \int_{\sum_{m=1}^{N} S_{H_m}} \Psi_s^e \frac{\partial G}{\partial n} ds \tag{31}$$

where Ψ_s^e, $\frac{\partial \Psi_s^e}{\partial n}$ are the scattered wave potential and normal derivative of the scattered wave potential on the boundary.

Once the incident wave potential and scattered wave potential are known then the pressure, the wave forces and run-up on the cylinders can be calculated.

2.5 Formulation of Wave Force

The wave pressure acting on the cylinder is defined as follows:

$$P(x, y, z; t) = R_e[\, p(x, y, z) e^{-i\sigma t}\,] \tag{32}$$

The Bernoulli equation is used to get the wave pressure:

$$p(x, y, z) = i\sigma\rho\phi(x, y, z) \tag{33}$$

where ρ is the water density.

The wave pressure is presented by using Ψ_i, Ψ_s as follows:

$$p = \rho g \frac{H}{2} \frac{\cosh k(z+h)}{\cosh kh} (\Psi_i + \Psi_s) \tag{34}$$

The wave force in j direction acting on the cylinder mth is defined as follows:

$$F_j^m = R_e[\, f_j^m e^{-i\sigma t}\,] \tag{35}$$

The wave force in j direction is presented by using Ψ_i, Ψ_s as follows:

$$f_j^m = \rho g \frac{H}{2} \int_{-h}^{0} \frac{\cosh k(z+h)}{\cosh kh} dz \int_{S_{Hm}} (\Psi_i + \Psi_s) n_j ds \tag{36}$$

Finally, by integrating the wave force in z direction, the total wave force on the cylinder is defined as follows:

$$f_j^m = \rho g \frac{H}{2} \frac{\tanh kh}{k} \int_{S_{Hm}} (\Psi_i + \Psi_s) n_j ds \tag{37}$$

Also the moment M_j^m in j direction on the cylinder mth is defined as follows:

$$M_j^m = \rho g \frac{H}{2} h^2 \left\{ \frac{kh\sinh(kh) + 1 - \cosh(kh)}{(kh)^2 \cosh(kh)} \right\} \times \int_{S_{Hm}} (\Psi_i + \Psi_s) n_j ds \tag{38}$$

where n_j is the normal vector in the j direction element.

2.6 Formulation of Wave Run-up

The free-surface elevation is given by:

$$\eta(x, y; t) = R_e[\bar{\eta}(x, y) e^{-i\sigma t}] \qquad \text{on } z = 0 \tag{39}$$

where $\bar{\eta}(x, y)$ is presented by using Ψ_i, Ψ_s as follows:

$$\bar{\eta}(x, y) = \frac{H}{2} (\Psi_i + \Psi_s) \tag{40}$$

Chapter 3

DISCRETIZATION OF INTEGRAL EQUATION

3.1 Discretization of the Boundary

To approximate the geometry, the surfaces of the cylinders are divided into N boundary elements $\Delta_i (i = 1,2..N)$. Inside each element Δ_i, the potential ϕ_s and the normal derivative of velocity potential $\frac{\partial \phi_s}{\partial n}$ are interpolated using the shape function and the node values. Therefore, the integral equation (24) leads to:

$$\frac{1}{2}\phi_s(P_i) + \sum_{j=1}^{N} \phi_s(P_j) \int\int_{\Delta_j} \frac{\partial G(P_i, Q)}{\partial n} ds = \sum_{j=1}^{N} \frac{\partial \phi_s(P_j)}{\partial n} \int\int_{\Delta_j} G(P_i, Q) ds \qquad (41)$$

where P_i, P_j are the coordinate of the points located in the middle of element ith and jth respectively.

In two dimensional boundary value problems (Fig. 5), the surfaces of the cylinders S_{H_m} are divided into N boundary elements $\Delta_i (i = 1,2..N)$. The integral equation Eq. (30) leads to:

$$\frac{1}{2}\Psi_s(P_i) + \sum_{j=1}^{N} \Psi_s(P_j) \int_{\Delta_j} \frac{\partial G(P_i, Q)}{\partial n} ds = \sum_{j=1}^{N} \frac{\partial \Psi_s(P_j)}{\partial n} \int_{\Delta_j} G(P_i, Q) ds \qquad (42)$$

3.2 The Collocation Method

The collocation method allows calculate the unknown boundary data from Eq. (42). The principle of collocation means to locate the load point sequentially at nodes of all the elements of the boundary such that the variable at the observation point coincides with the nodal value.

By collocating the observation point i with the nodes 1 to N of the elements of the boundary, we can write Eq. (42) in matrix notation as follows:

$$\begin{pmatrix} \hat{G}_{11} & \hat{G}_{12} & \cdots & \hat{G}_{1N} \\ \hat{G}_{21} & \hat{G}_{22} & \cdots & \hat{G}_{2N} \\ \vdots & \vdots & \ddots & \vdots \\ \hat{G}_{N1} & \hat{G}_{N2} & \cdots & \hat{G}_{NN} \end{pmatrix} \cdot \begin{pmatrix} \Psi_s(P_1) \\ \Psi_s(P_2) \\ \vdots \\ \Psi_s(P_N) \end{pmatrix} = \begin{pmatrix} G_{11} & G_{12} & \cdots & G_{1N} \\ G_{21} & G_{22} & \cdots & G_{2N} \\ \vdots & \vdots & \ddots & \vdots \\ G_{N1} & G_{N2} & \cdots & G_{NN} \end{pmatrix} \cdot \begin{pmatrix} \hat{\Psi}_s(P_1) \\ \hat{\Psi}_s(P_2) \\ \vdots \\ \hat{\Psi}_s(P_N) \end{pmatrix} \quad (43)$$

In Eq. (43) the matrix element $\hat{G}_{ij}$ and G_{ij} is defined as follows:

$$\hat{G}_{ij} = \begin{cases} \frac{1}{2} + \int_{\Delta_j} \frac{\partial G(P_i, Q)}{\partial n} ds & (i = j) \\ \int_{\Delta_j} \frac{\partial G(P_i, Q)}{\partial n} ds & (i \neq j) \end{cases} \quad (44)$$

and $$G_{ij} = \int_{\Delta_j} G(P_i, Q) ds \quad (45)$$

Also in Eq. (43), on the left hand side $\Psi_s(P_i)$ is the velocity potential value of scattered wave at the node P_i of element i, and on the right hand side $\hat{\Psi}_s(P_i)$ is normal derivative value of velocity potential of scattered wave at the node P_i of element i.

3.3 Calculation of Matrix Element

On the left-hand side of Eq. (43), $\hat{G}_{ij}$ is the derivative of Green function respect to the normal drawn outwardly vector $\vec{n}$ on the boundary and is defined as $\partial G / \partial n$. Also, on the right-hand side, $\hat{\Psi}_s$ is the derivative of velocity potential of scattered wave respect to the normal drawn outwardly vector $\vec{n}$ on the boundary and is defined as $\partial \Psi_s / \partial n$. If the unit normal vector component n_x, n_y, n_z is used, $\partial G / \partial n$ and $\partial \Psi_s / \partial n$ are defined as follows:

$$\frac{\partial G}{\partial n} = n_x \frac{\partial G}{\partial x} + n_y \frac{\partial G}{\partial y} + n_z \frac{\partial G}{\partial z} \quad (46)$$

$$\frac{\partial \Psi_s}{\partial n} = n_x \frac{\partial \Psi_s}{\partial x} + n_y \frac{\partial \Psi_s}{\partial y} + n_z \frac{\partial \Psi_s}{\partial z} \quad (47)$$

In two dimensional $x - y$ plane, $\partial G / \partial n$ and $\partial \Psi_s / \partial n$ are defined as follows:

$$\frac{\partial G}{\partial n} = n_x \frac{\partial G}{\partial x} + n_y \frac{\partial G}{\partial y} \quad (48)$$

$$\frac{\partial \Psi_s}{\partial n} = n_x \frac{\partial \Psi_s}{\partial x} + n_y \frac{\partial \Psi_s}{\partial y} \tag{49}$$

where $\partial G/\partial x, \partial G/\partial y, \partial G/\partial z$ are the derivative of Green function respect to x, y and z. $\partial \Psi_s/\partial x, \partial \Psi_s/\partial y$, $\partial \Psi_s/\partial z$ are the derivative of scattered velocity potential respect to x, y and z respectively.

To calculate coefficients $\hat{G}_{ij}$ and G_{ij} in Eq. (44) and Eq. (45), the integral equations can be approximated as follows:

$$\int_{\Delta_j} G(P_i, Q) ds \cong G(P_i, P_j)\Delta_j \tag{50}$$

$$\int_{\Delta_j} \frac{\partial G(P_i, Q)}{\partial n} ds \cong \frac{\partial G(P_i, P_j)}{\partial n}\Delta_j \tag{51}$$

where Δ_j is the area of the element j.

3.4 Derivation of Green Function

Green function is the function which satisfies the boundary conditions Eqs.(14)~(17). The eigenfunction expansion satisfies the free surface boundary condition Eq. (15) and sea bed boundary condition Eq. (16) is defined as follows:

$$\phi_n(z) = \begin{cases} \sqrt{\dfrac{2k_0^2}{h(k_0^2 - \nu^2) + \nu)}} \dfrac{\cosh k_0(h+z)}{\cosh k_0 z} & (\text{for } n = 0) \\ \sqrt{\dfrac{2k_n^2}{h(k_n^2 - \nu^2) + \nu)}} \dfrac{\cosh k_n(h+z)}{\cosh k_n z} & (\text{for } n = 1, 2, ...) \end{cases} \tag{52}$$

The Delta function can be expanded as follows:

$$\delta(z - \zeta) = \sum_{n=0}^{\infty} \phi_n(z)\hat{\phi}_n(\zeta) \tag{53}$$

where $\hat{\phi}_n$ is the conjugate function of ϕ_n.

The Green function G is supposed as follows:

$$G(P, Q) = \sum_{n=0}^{\infty} G_n(x, y, \xi, \eta)\phi_n(z)\hat{\phi}_n(\zeta) \tag{54}$$

By substituting Eq. (54) into left hand side of basic equation (14) and substituting Eq. (53) into the right hand side, the result is obtained as follows:

$$\sum_{n=0}^{\infty}(\nabla^2 G_n \pm k_n^2 G_n)\phi_n(z)\hat{\phi}_n(\zeta) = -\sum_{n=0}^{\infty}\delta(x-\xi)\delta(y-\eta)\phi_n(z)\hat{\phi}_n(\zeta) \qquad (55)$$

where ∇^2 is the Laplace operator. In the parentheses, as $n=0$ the double sign is plus sign (+) and as $n=1,2...$ the double sign is minus sign (-).

Therefore, the Green function, $G_n(n=0,1,2...)$, need to satisfy condition as follows:

$$\nabla^2 G_n \pm k_n^2 G_n = -\delta(x-\xi)\delta(y-\eta) \qquad (56)$$

Eq. (56) is the two dimensional Helmholtz equation as $n=0$, and is the modified the two dimensional Helmholtz equation as $n=1,2...$

The fundamental solution for Helmholtz equation is obtained as follows:

$$G(x,y;\xi,\eta) = \begin{cases} \dfrac{i}{4}H_0^{(1)}(k_0 R) & (n=0) \\ \dfrac{1}{2\pi}K_0(k_n R) & (n=0,1,2...) \end{cases} \qquad (57)$$

$$R = \sqrt{(x-\xi)^2 + (y-\eta)^2}$$

where, $H_0^{(1)}$ denote the Hankel function of the first kind and order zero, K_0 denote the modified Bessel function of the second kind and order zero.

Substituting Eq. (57) into Eq. (54) and using the eigenfunction, $\phi_n(n=0,1,2...)$, the three- dimensional Green function of wave motion can be derived as follows:

$$G(P,Q) = i\frac{k_0^2\cosh(k_0(h+\zeta))\cosh(k_0(h+z))}{2\{h(k_0^2-\nu^2)+\nu\}\cosh(h^2 k_0 h)}H_0^{(1)}(k_0 R)$$

$$+\sum_{n=1}^{\infty}\frac{k_n^2\cos(k_n(h+\zeta))\cos k_0(h+z)}{\pi\{h(k_n^2+\nu^2)-\nu\}\cosh^2(k_n h)}K_0(k_n R) \qquad (58)$$

In which, $\cosh^2(k_0h)^{-1} = 1 - \tanh^2(k_0h)$ and $(\cosh^2 k_nh)^{-1} = 1 + \tanh^2(k_nh)$ and the dispersion relation $k_0 \tanh k_0h = \nu$ and $k_n \tanh k_nh = -\nu$. By substituting these coefficients into Eq. (58), the result is derived as follows:

$$G(P,Q) = i\frac{(k_0^2 - \nu^2)\cosh k_0(h+\zeta)}{2\{h(k_0^2 - \nu^2) + \nu\}}\cosh hk_0(h+z)H_0^{(1)}(k_0R)$$

$$+\sum_{n=1}^{\infty}\frac{(k_n^2 + \nu^2)\cos k_n(h+\zeta)}{\pi\{k_n(k_n + \nu^2) - \nu\}}\cosh k_n(h+z)K_0(k_nR) \qquad (59)$$

Chapter 4
NUMERICAL EXAMPLES

4.1 Wave Forces on Two Vertical Circular Cylinders

Fig. 6 demonstrates the geometries of two transverse cylinders and two tandem cylinders used in this study. The figure shows two cylinders, having radius $a_1 = a_2 = a$, subjected to incident wave comes from the left side. D is the distance between the centers of the cylinders. The wave exciting force on the cylinders, run-up and free-surface elevation around the cylinders $10a$ distance are calculated. In order to compare with the results of Chakrabarti (1978) and Ohkusu (1974), in all figures the wave forces are nondimensionalized by $\rho g(H/2)a^2$ and the magnitude of run-up and free-surface elevation are nondimensionalized by wave height H.

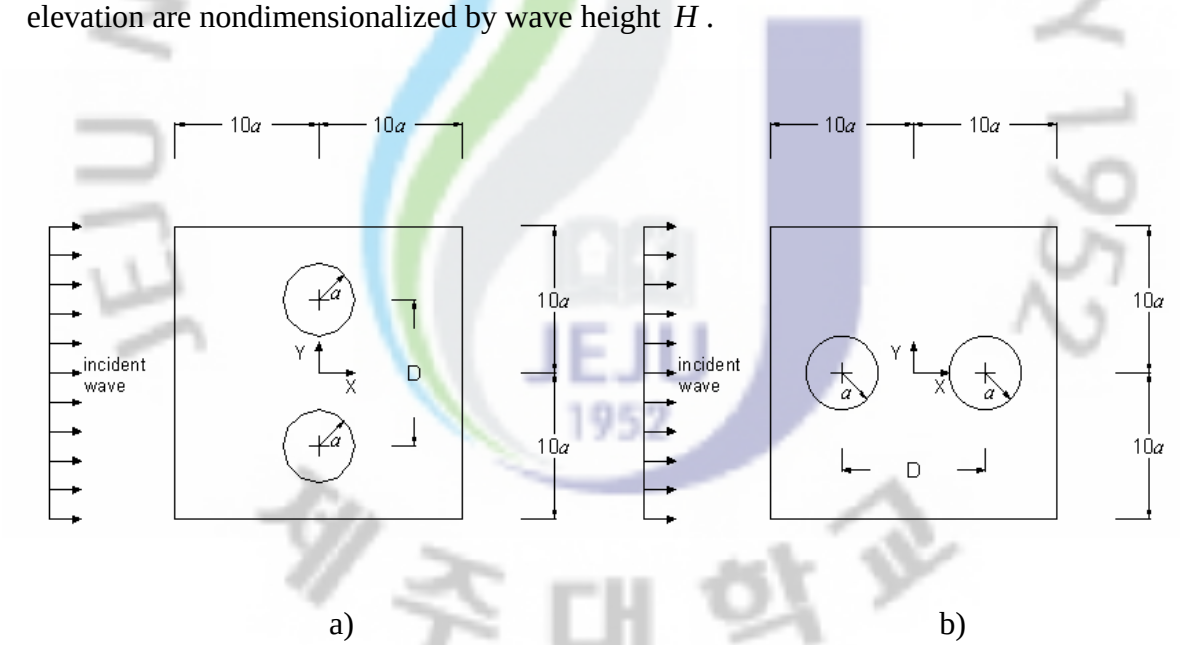

a) b)

Fig. 6 Geometries of: a) Two transverse cylinders; b) Two tandem cylinders

Fig. 7 and Fig. 8 show the wave forces in x-direction and y-direction acting on cylinder 1 in two transverse cylinders versus the wave number ka. Due to the symmetry of the geometry, the wave forces acting on cylinder 2 are the same. The wave forces acting on an isolate cylinder are also plotted for purpose of comparison. Fig. 7 shows that the wave forces on each cylinder in two transverse cylinders are higher than that on isolate cylinder because of the interaction of two cylinders. The numerical computation results of this study are strong agreement with those of Chakrabarti (1978).

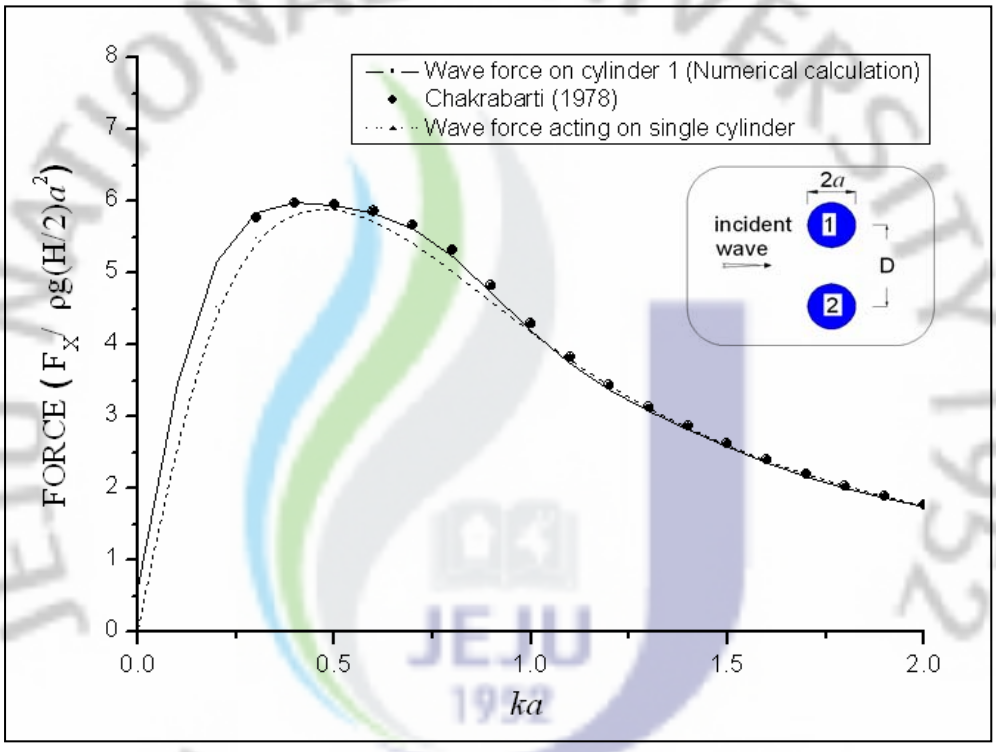

Fig. 7 Wave forces in x-direction acting on cylinder 1 in two transverse cylinders versus wave number ka for $D/a = 5$, $h/a = 10$

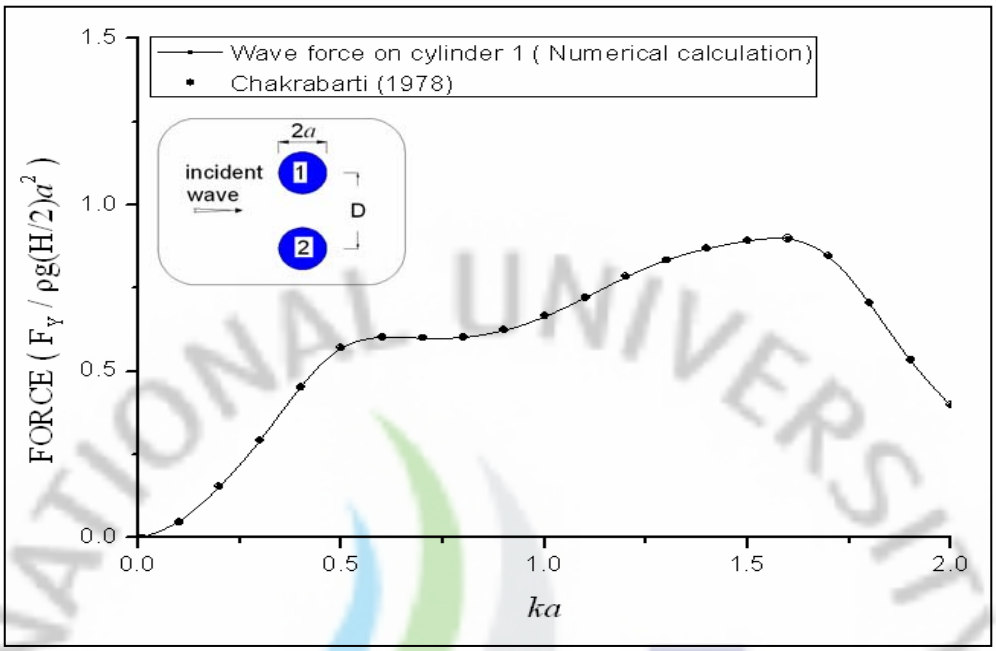

Fig. 8 Wave forces in y-direction acting on cylinder 1 two transverse cylinders versus wave number ka for $D/a = 5$, $h/a = 10$

Fig. 9 shows the wave forces in x-direction acting on the cylinders in two tandem cylinders versus the wave number ka. The wave forces in y-direction on the cylinders in two tandem cylinders are zero. The results in Fig. 9 show that the wave forces on two cylinders reach maximum values near $ka = 0.5$ and the variation of the wave force on the front cylinder is more than that on the back cylinder. In two tandem cylinders, the wave forces on the rear cylinder are reduced by the shielding effect. Also, Fig. 9 shows that the numerical computation results of this study are strong agreement with those of Ohkusu (1974).

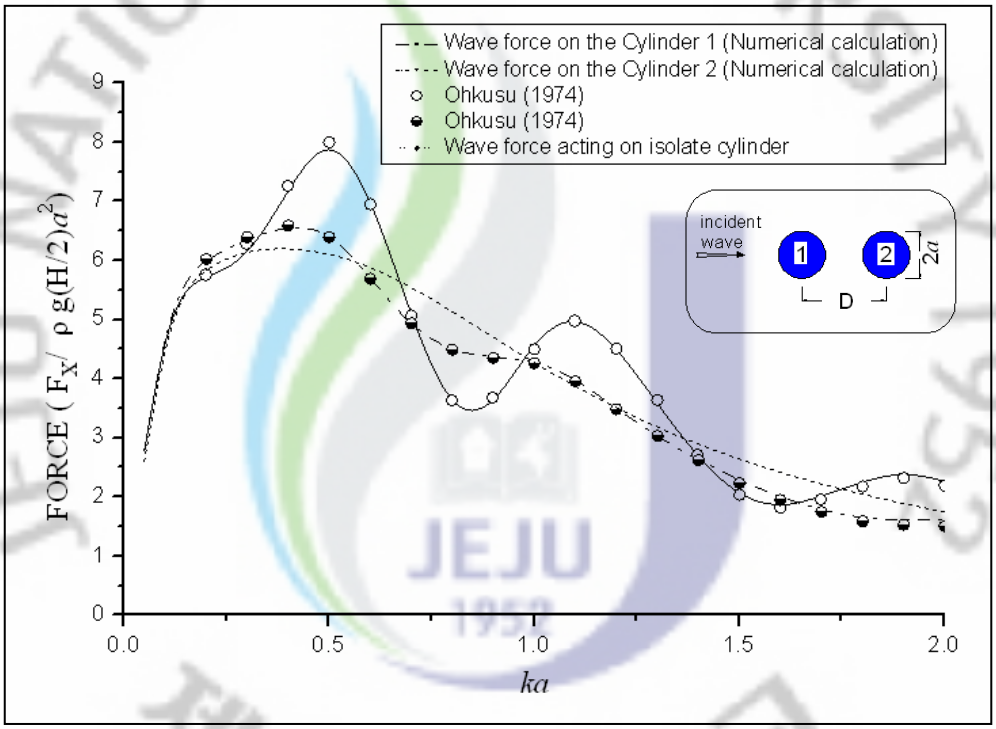

Fig. 9 Wave forces in x-direction acting on two tandem cylinders versus wave number ka for $D/a = 5$, $h/a = 10$

4.1.1 The Effects of Cylinder Spacing on Wave Forces on Two Vertical Circular Cylinders

The effects of the separation distance among two cylinders on the wave forces on two cylinders are also investigated in this study. Fig. 10 and Fig. 11 show the wave forces in x - direction and y - direction acting on each cylinder in two transverse cylinders versus the ratio $\gamma = 2a/D$ for three special wave numbers $ka = 0.1, 0.5, \text{and } 1.0$. In which, a is the radius of the cylinders, and D is the distance between the centers of the cylinders. In this geometry, $\gamma = 1$ represents that the cylinders are touching each other, whereas $\gamma = 0$ represents that the distance between two cylinder centers $D \to \infty$. Due to the symmetry of the geometry, the wave forces in x - direction and y - direction acting on each cylinder 1 and cylinder 2 are the same.

Fig. 12 shows the wave forces in x - direction acting on the cylinders in two tandem cylinders versus the ratio $\gamma = 2a/D$ for three special wave numbers $ka = 0.1, 0.5, \text{and } 1.0$. The wave force in y - direction is zero due to the symmetry of the geometry. In all figures, the corresponding wave forces acting on isolated cylinder are also plotted for the purpose of comparison.

From the results shown in Fig. 10 to Fig. 12, as the cylinder spacing increases, the wave forces on the cylinders do not decrease linear to the wave forces on an isolated cylinder, however it oscillates around the wave forces on an isolated cylinder. The amplitude of oscillation is extremely large as the ratio $\gamma \geq 0.2$. As the cylinder spacing approaches infinity, the wave forces on the cylinders reach the wave force amplitude on an isolated cylinder.

Fig. 12 shows that the wave forces on the rear cylinder are extremely less than the wave forces on the front cylinder because of the shielding effect.

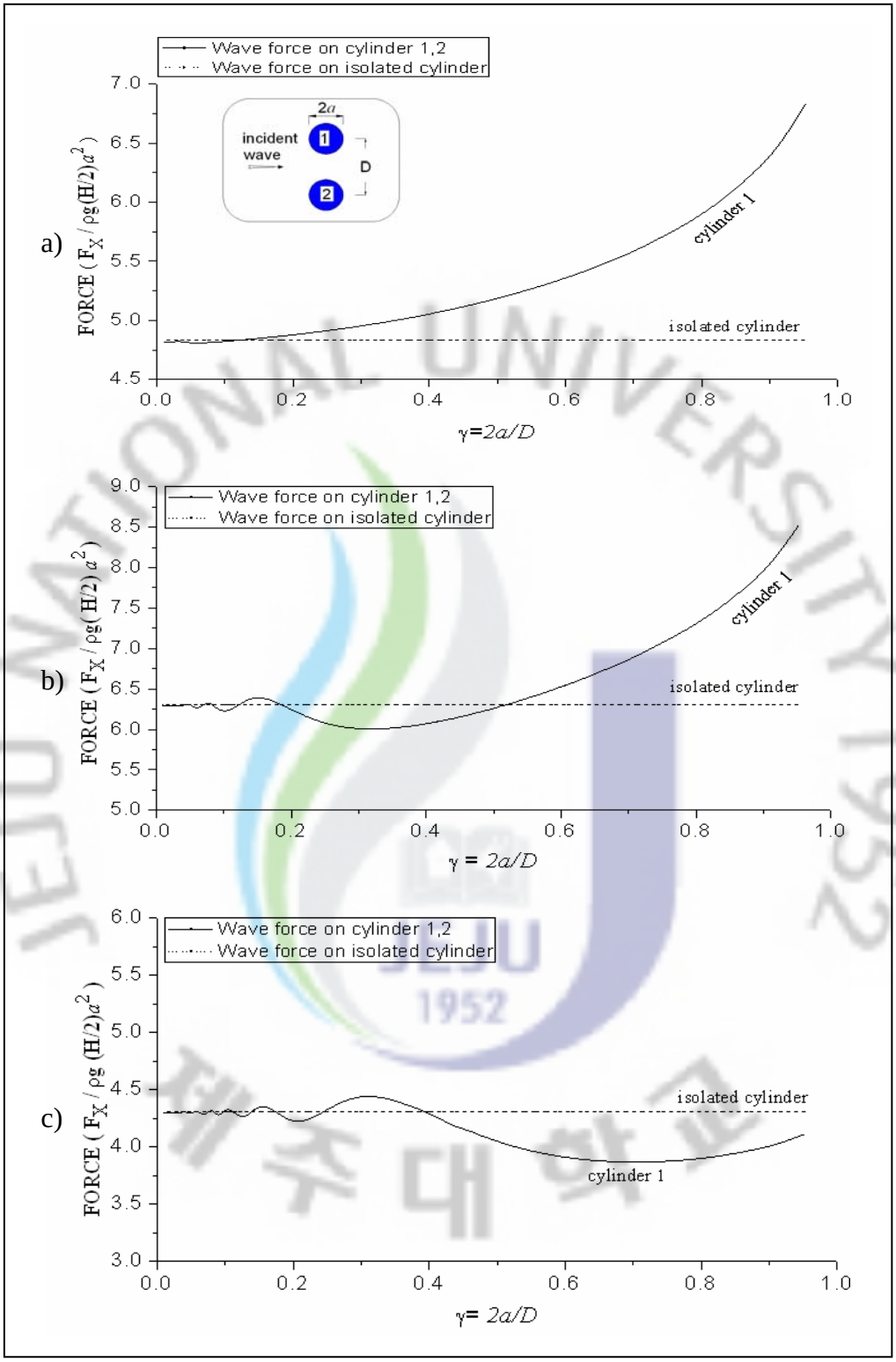

Fig. 10 Wave forces in x-direction acting on two transverse cylinders versus ratio $\gamma = 2a/D$ for $h/a = 10$: a) wave number $ka = 0.1$; b) wave number $ka = 0.5$; c) wave number $ka = 1.0$

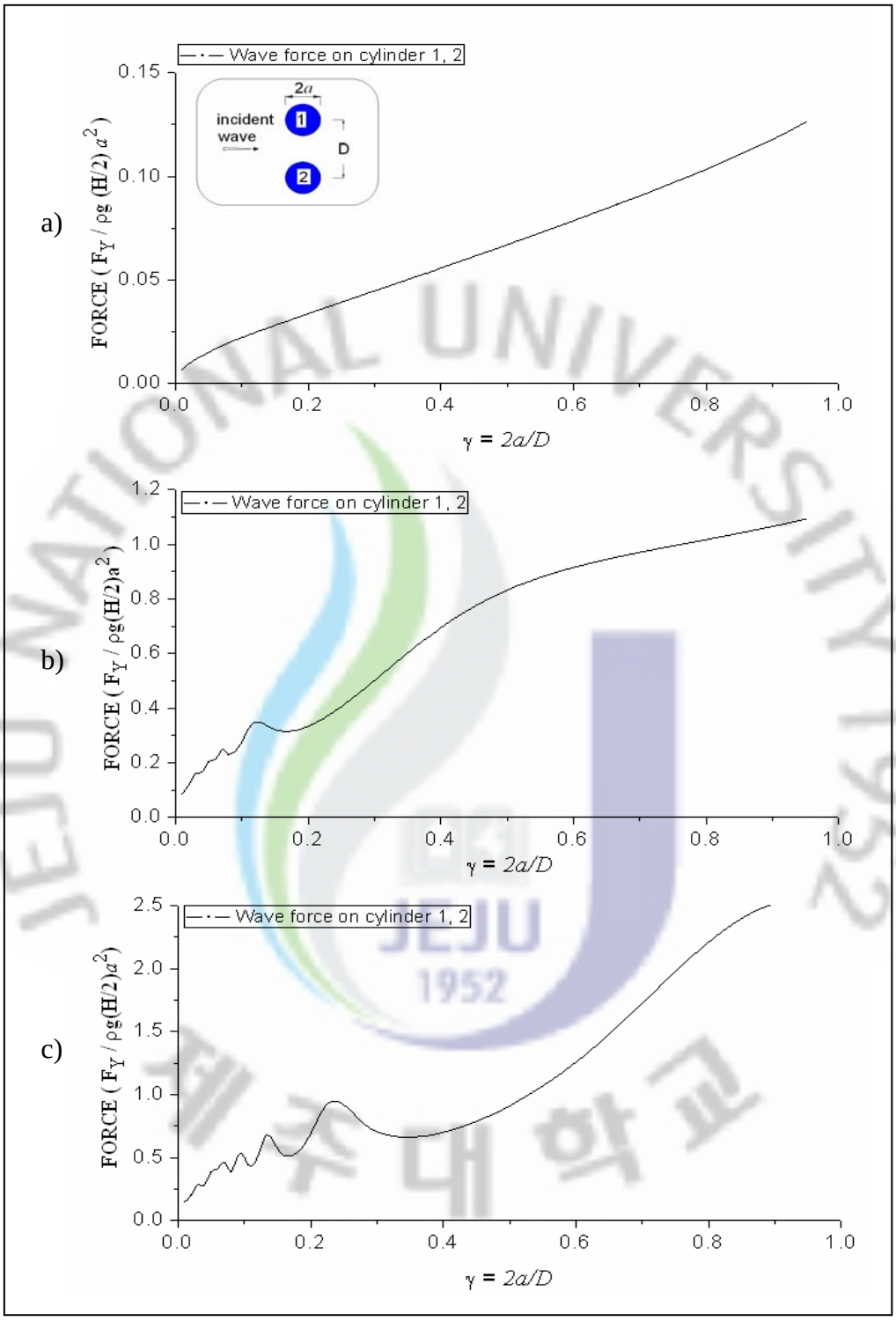

Fig. 11 Wave forces in y-direction acting on two transverse cylinders versus ratio $\gamma = 2a/D$ for $h/a = 10$: a) wave number $ka = 0.1$; b) wave number $ka = 0.5$; c) wave number $ka = 1.0$

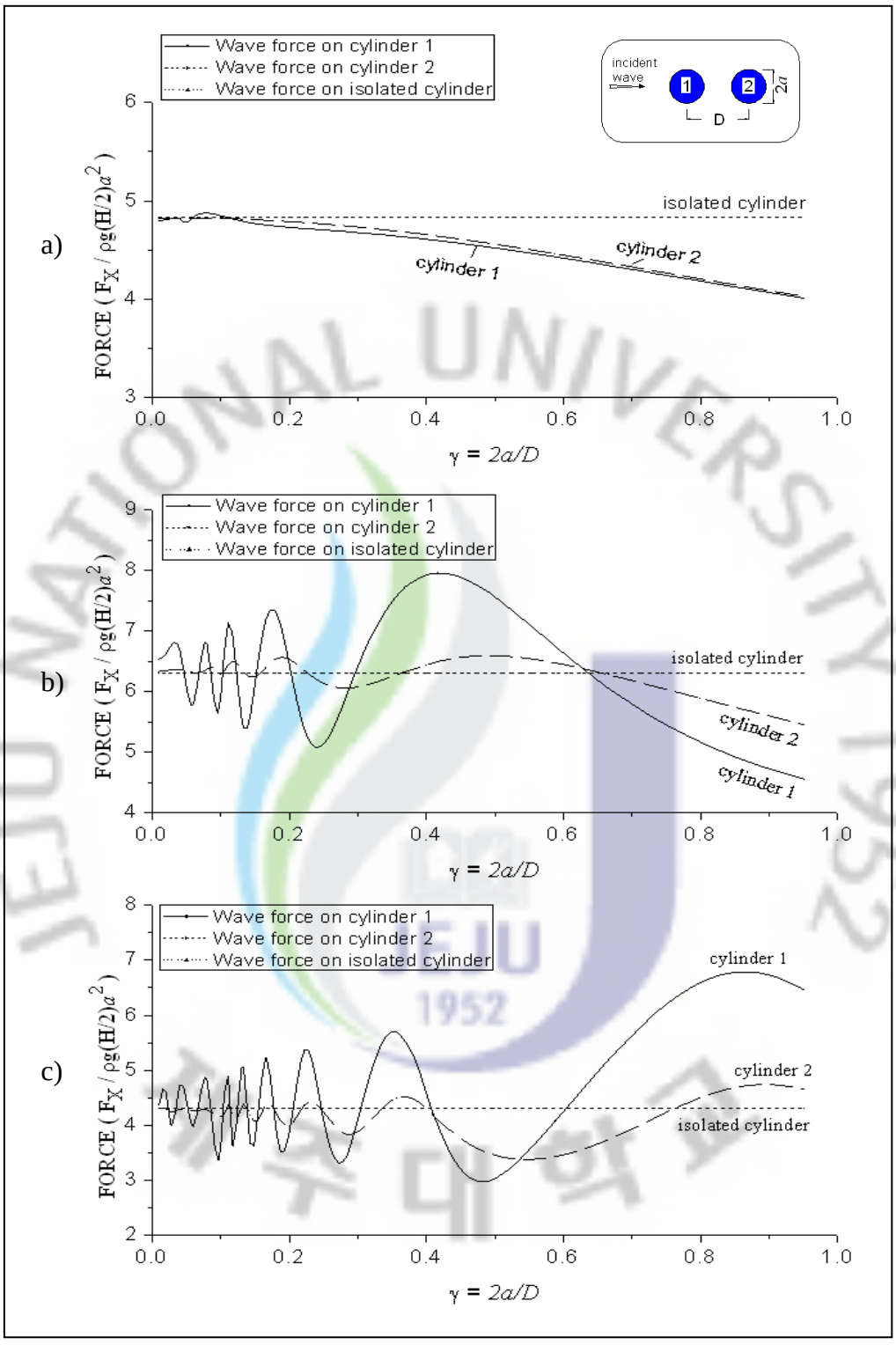

Fig. 12 Wave forces in x-direction acting on two tandem cylinders versus ratio $\gamma = 2a/D$ for $h/a = 10$: a) wave number $ka = 0.1$; b) wave number $ka = 0.5$; c) wave number $ka = 1.0$

4.1.2 The Effects of Position of the Cylinders on Wave Forces on Two Vertical Circular Cylinders

The effects of the position of the cylinders on the wave forces are also investigated in this study. Fig.13 shows the wave forces on the cylinders versus the variation of angle φ for special wave number $k = 0.5$, $D/a = 5$, $h/a = 10$. In which, φ is the counter-clockwise angle among the line joining the two cylinder centers and the x-axis. It can be seen from Fig. 13 that the maximum wave forces on the front cylinder as the angle φ is zero (two tandem cylinders) and it tend to decrease as the angle φ increases from $0 < \varphi < 90^o$.

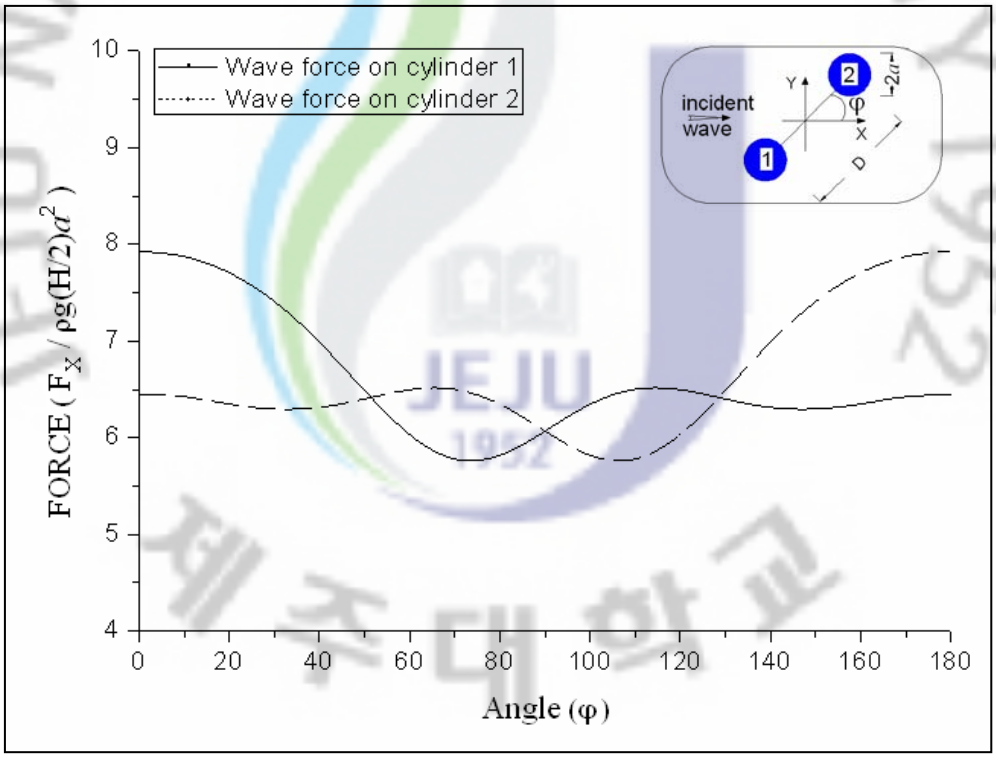

Fig. 13 Wave forces in x-direction acting on two cylinders versus ratio φ for $ka = 0.5$, $h/a = 10$, $D/a = 5$

4.1.3 The Effects of Incident Wave Angle on Wave Forces on Two Vertical Circular Cylinders

When incident wave is propagating at various angles $\beta = 0^0, 30^0, 45^0, 60^0$, the wave forces acting on the cylinders in two transverse cylinders and two tandem cylinders are computed as shown in Fig. 14 to Fig. 17. From the numerical computation results, the wave forces on the cylinders tend to decrease gradually as the incident wave angle increases in both two geometries. The variation of the wave forces on the cylinders in two tandem cylinders is larger than that on the cylinders in two transverse cylinders.

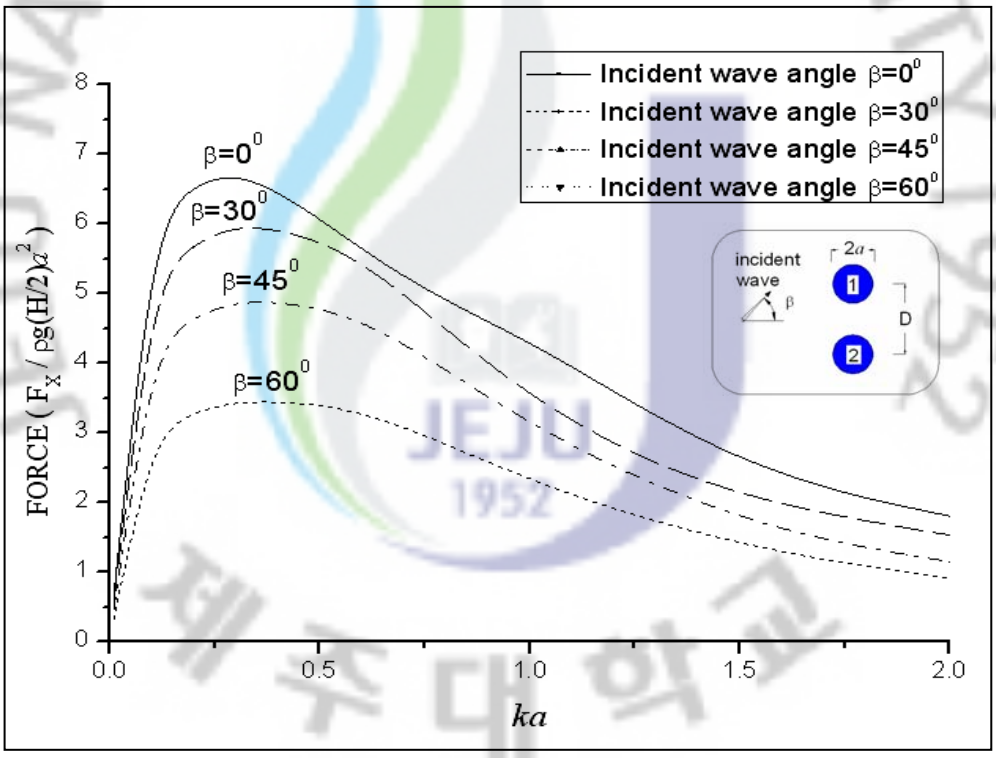

Fig. 14 Wave forces in x-direction acting on cylinder 1 in two transverse cylinders with four different incident wave angles $\beta = 0^0, 30^0, 45^0, 60^0$ for $h/a = 10, D/a = 5$

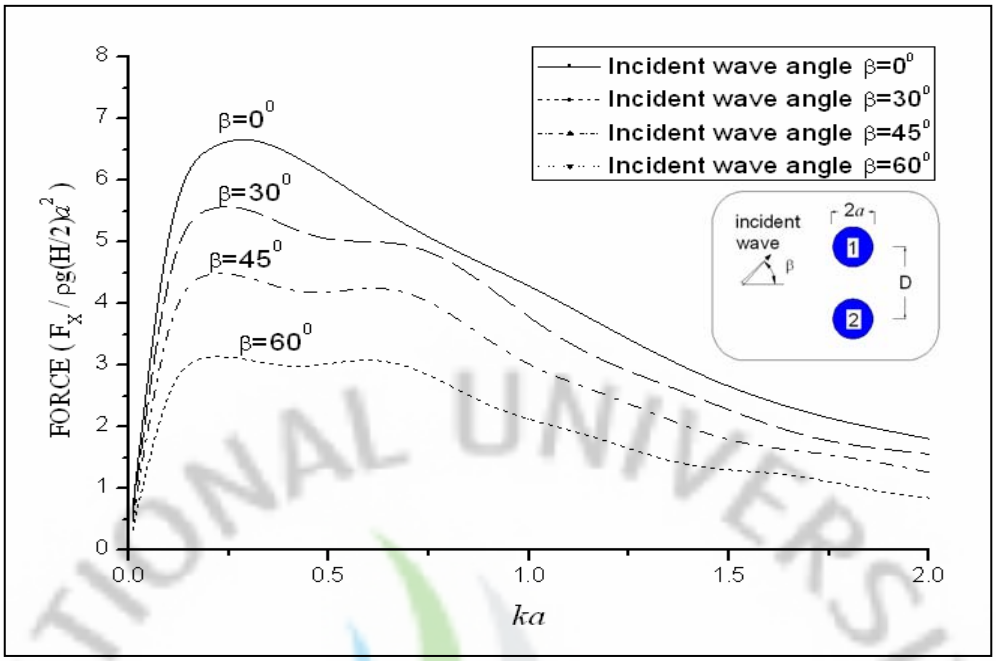

Fig. 15 Wave forces in x-direction acting on cylinder 2 in two transverse cylinders with four different incident wave angles $\beta = 0^0, 30^0, 45^0, 60^0$ for $h/a = 10, D/a = 5$

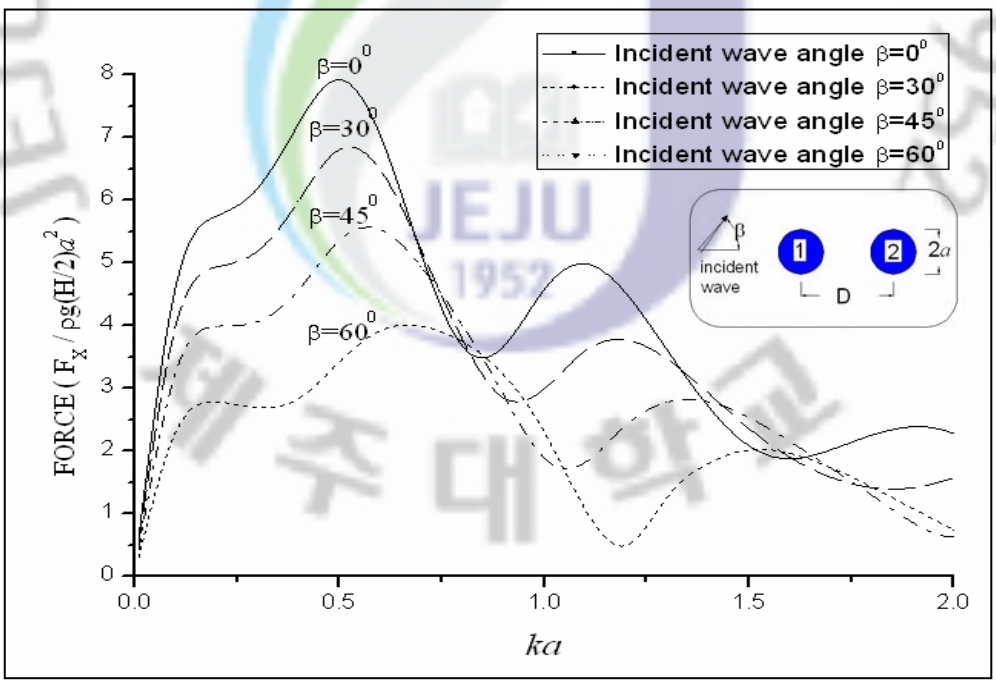

Fig. 16 Wave forces in x-direction acting on cylinder 1 in two tandem cylinders with four different incident wave angles $\beta = 0^0, 30^0, 45^0, 60^0$ for $h/a = 10, D/a = 5$

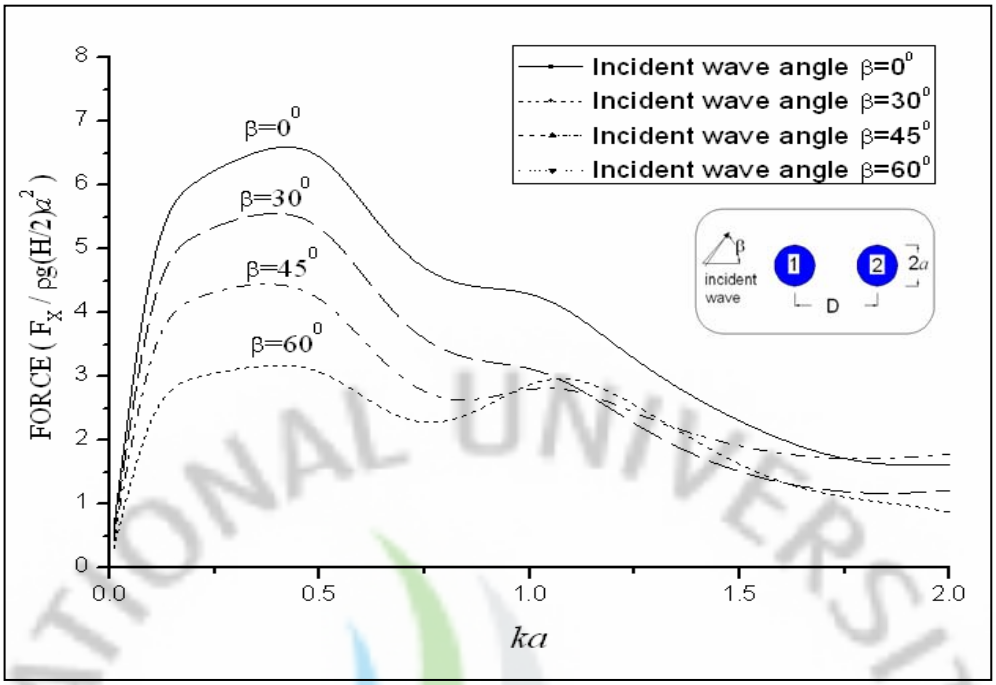

Fig. 17 Wave forces in x-direction acting on cylinder 2 in two tandem cylinders with four different incident wave angles $\beta = 0^0, 30^0, 45^0, 60^0$ for $h/a = 10$, $D/a = 5$

4.1.4 Run-up on the Outer Walls of Two Vertical Circular Cylinders

The numerical computation results of run-up on the outer walls of the cylinders in two transverse and two tandem cylinders are shown in Fig. 18 and Fig. 19. The computation results show that due to the interaction of the cylinders, the run-up profiles of the cylinders are quite different from that of an isolated cylinder. In two tandem cylinders, the run-up on the front cylinder is higher than that on the back cylinder because the shielding effect. Also, the numerical computation results have strong agreement with those of Chakrabarti (1978).

Fig. 20 to Fig. 23 present the run-up on the outer walls of the cylinders in two transverse cylinders and two tandem cylinders for $D/a = 5$, h/a=10, $ka = 1.0$ at four different incident wave angles $\beta = 0^{o}, 30^{o}, 45^{o}$, and 60^{o}.

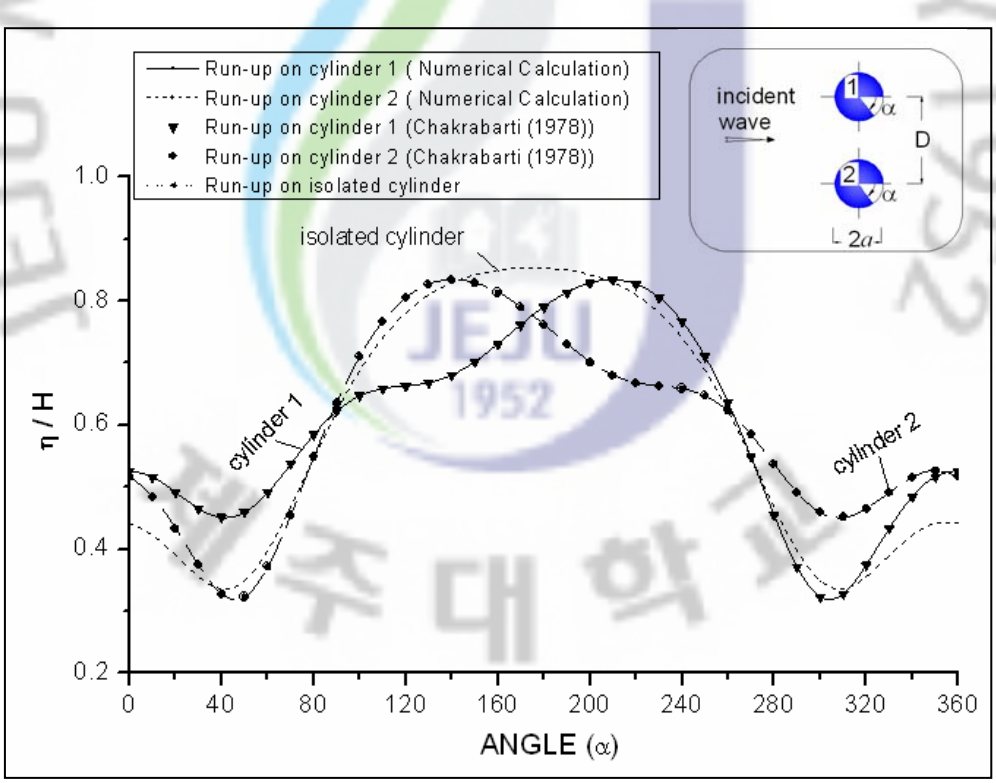

Fig. 18 Run-up on the outer walls of the cylinders in two transverse cylinders for $h/a = 10, D/a = 5, ka = 1.0$

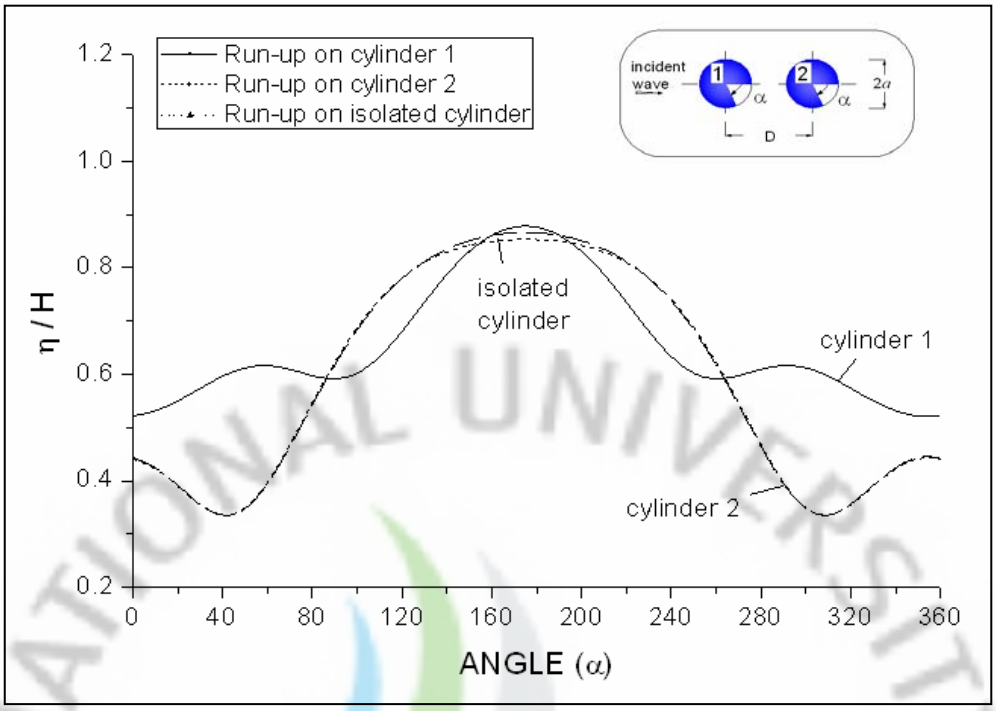

Fig. 19 Run-up on the outer walls of the cylinders in two tandem cylinders for $h/a=10, D/a=5, ka=1.0$

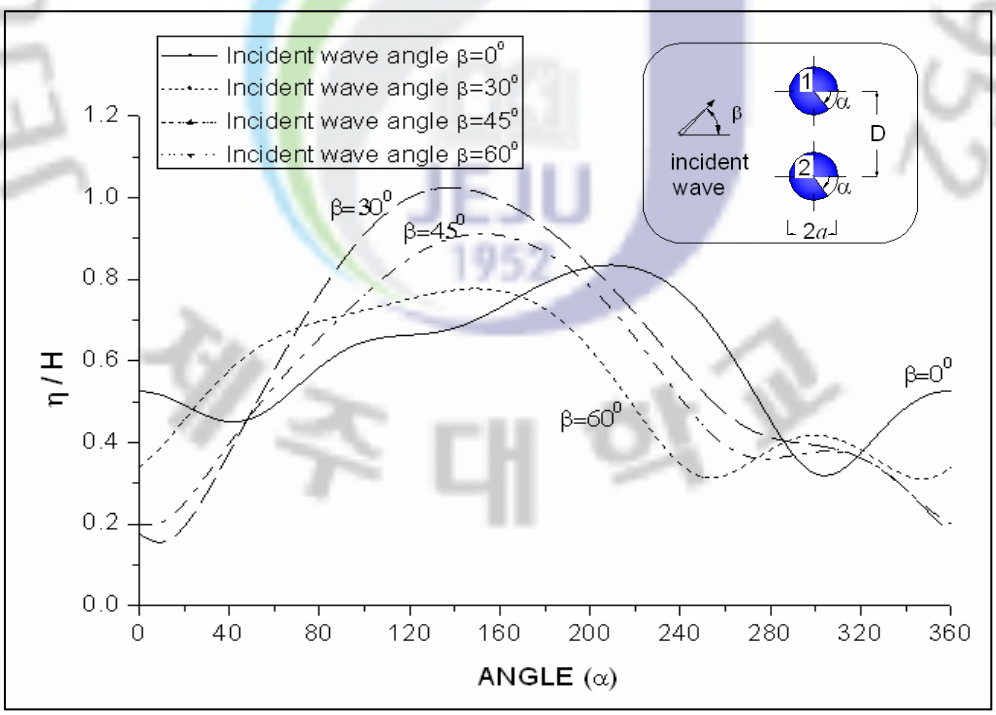

Fig. 20 Run-up on the outer walls of cylinder 1 in two transverse cylinders versus incident wave angle β **for** $h/a=10, D/a=5, ka=1.0$

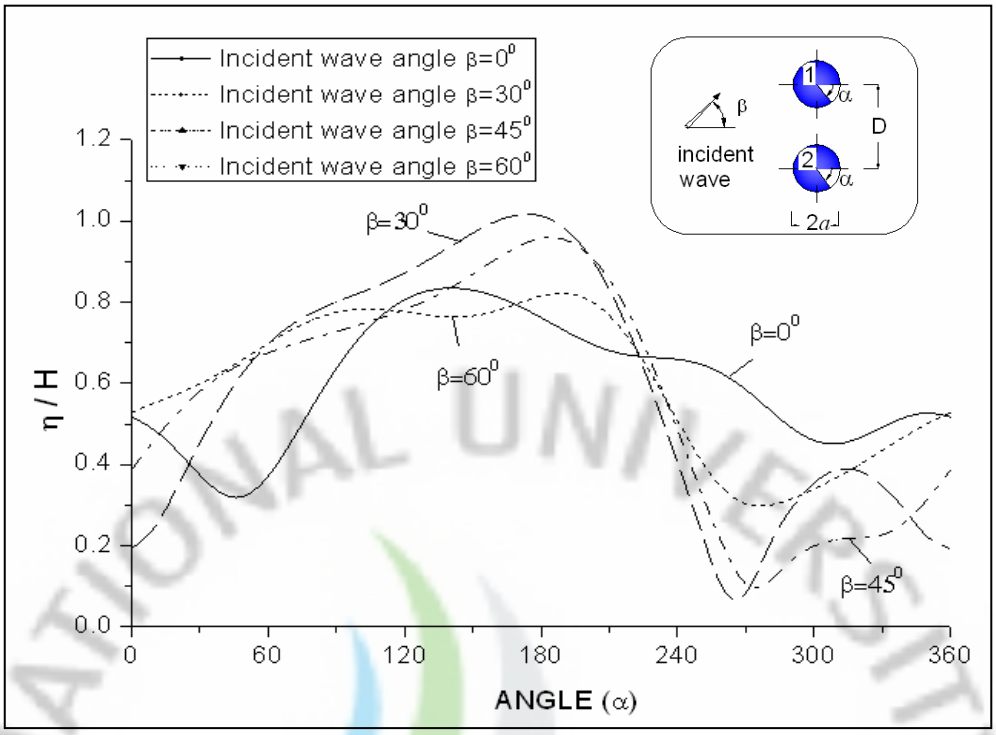

Fig. 21 Run-up on the outer walls of cylinder 2 in two transverse cylinders versus incident wave angle β for $h/a=10, D/a=5, ka=1.0$

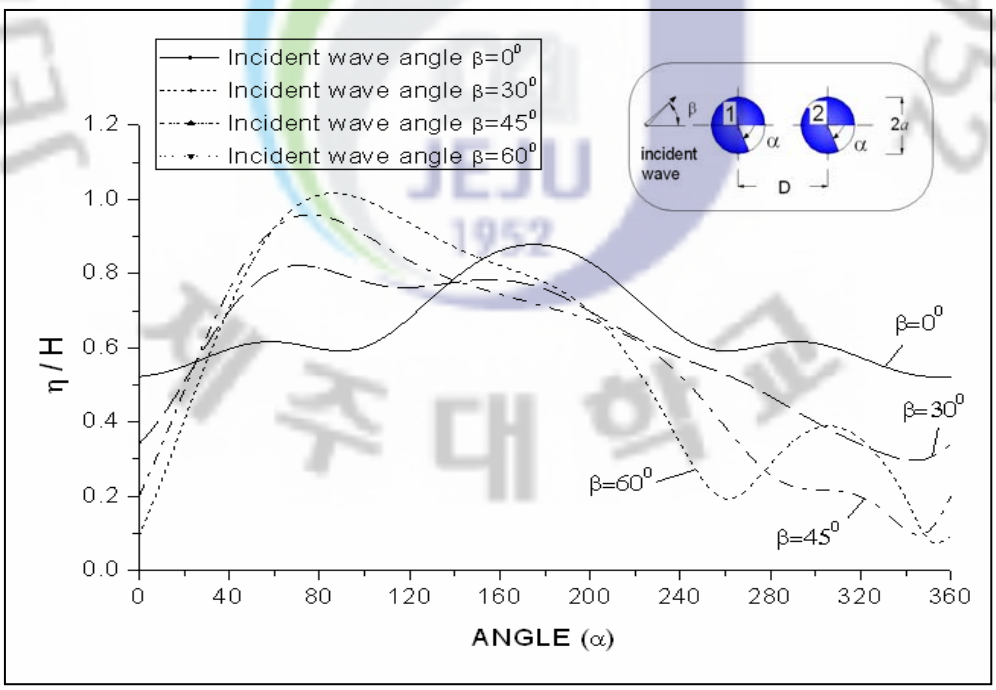

Fig. 22 Run-up on the outer walls of cylinder 1 in two tandem cylinders versus incident wave angle β for $h/a=10, D/a=5, ka=1.0$

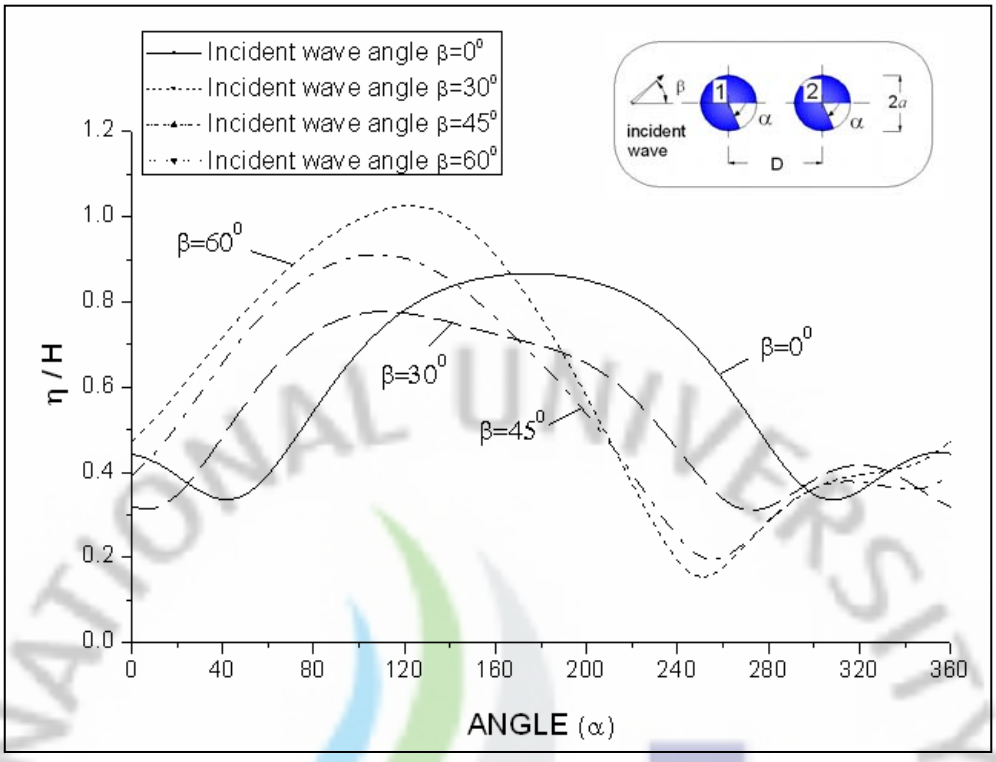

Fig. 23 Run-up on the outer walls of cylinder 2 in two tandem cylinders versus incident wave angle β for $h/a=10, D/a=5, ka=1.0$

4.1.5 Free-Surface Elevation around Two Vertical Circular Cylinders

The free-surface elevation contour around two transverse cylinders and two tandem cylinders for special wave number $ka = 1.0$ and incident wave angle $\beta = 0^0$ is computed as shown in Fig. 24 and Fig. 26. The run-up on the cylinders in Fig. 18 and Fig. 19 is presented by the same value as in Fig. 24 and Fig. 26.

Fig. 25 and Fig. 27 show the wave height distribution around two transverse and two tandem cylinders using three-dimensional graphic technique.

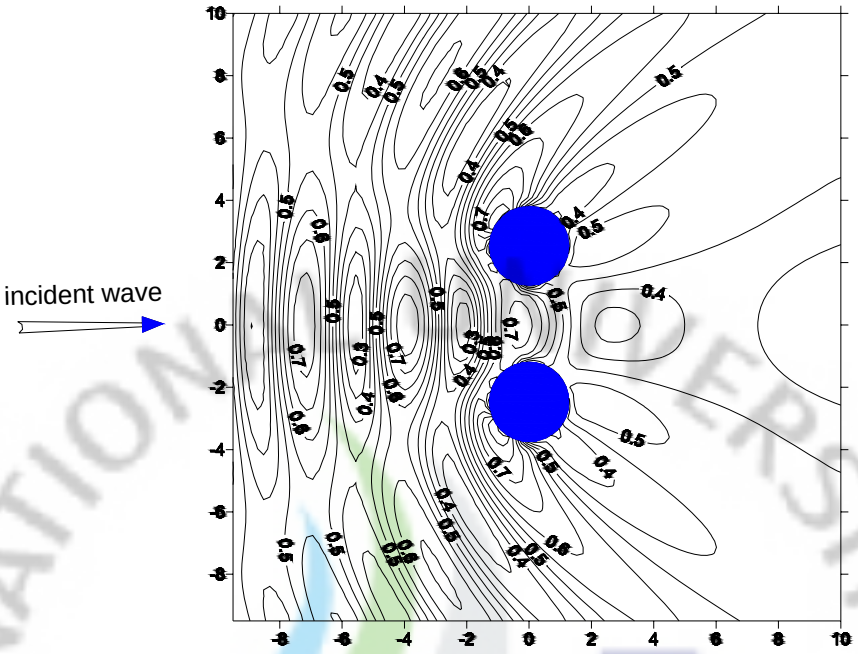

Fig. 24 Free-surface elevation contour around two transverse cylinders for $h/a=10, D/a=5, ka=1.0$

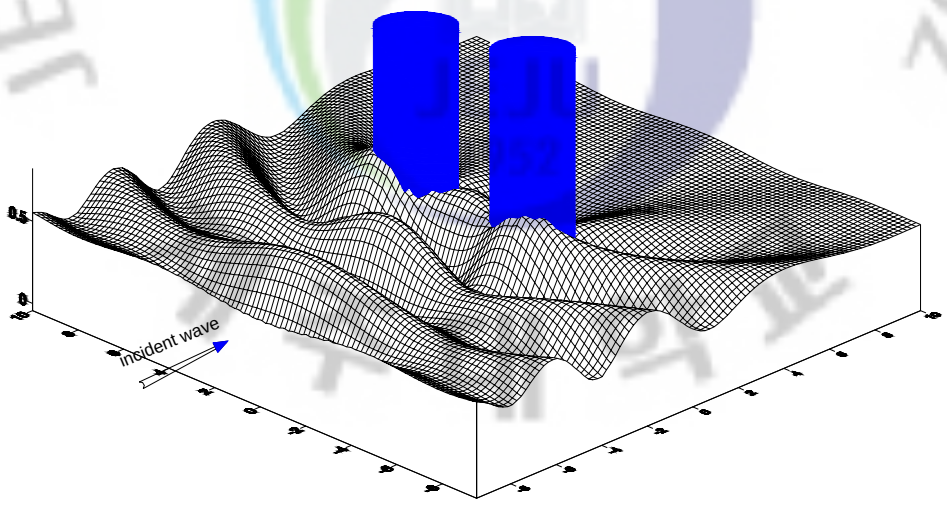

Fig. 25 Wave height distribution around two transverse cylinders using three-dimensional graphic technique for $h/a=10, D/a=5, ka=1.0$

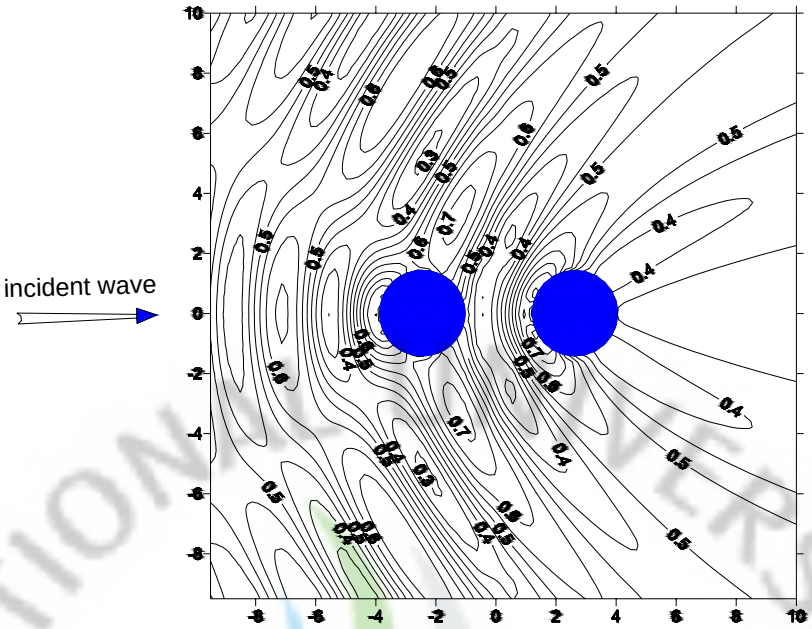

Fig. 26 Free-surface elevation contour around two tandem cylinders for $h/a=10, D/a=5, ka=1.0$

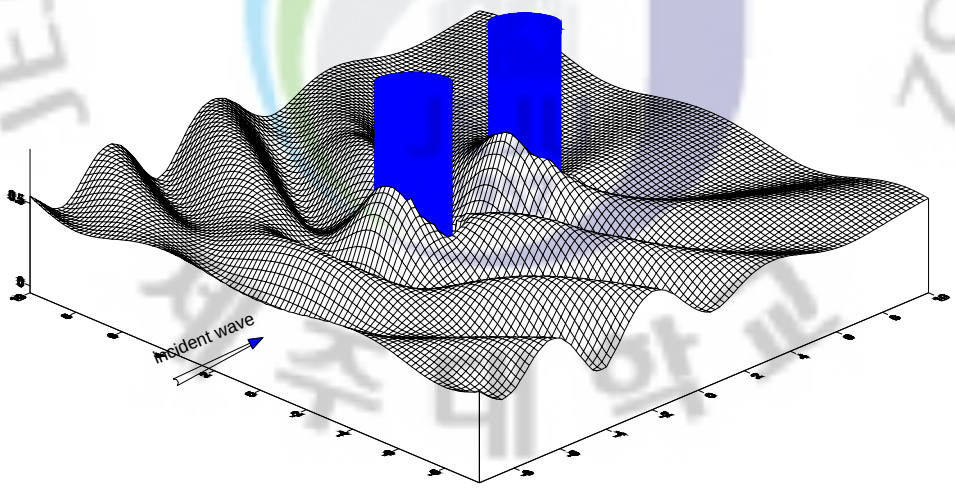

Fig. 27 Wave height distribution around two tandem cylinders using three-dimensional graphic technique for $h/a=10, D/a=5, ka=1.0$

4.2 Wave Forces on Three Vertical Circular Cylinders

Fig. 28 demonstrates the geometries of three vertical circular cylinders used in this study. The figure shows three cylinders, having radius $a_1 = a_2 = a_3 = a$, subjected to the incident waves come from the left side. Three different geometries of three cylinders are used in this study: triangular array, row array and column array. The wave forces, run-up and free-surface elevation around three cylinders 10*a* distance are calculated.

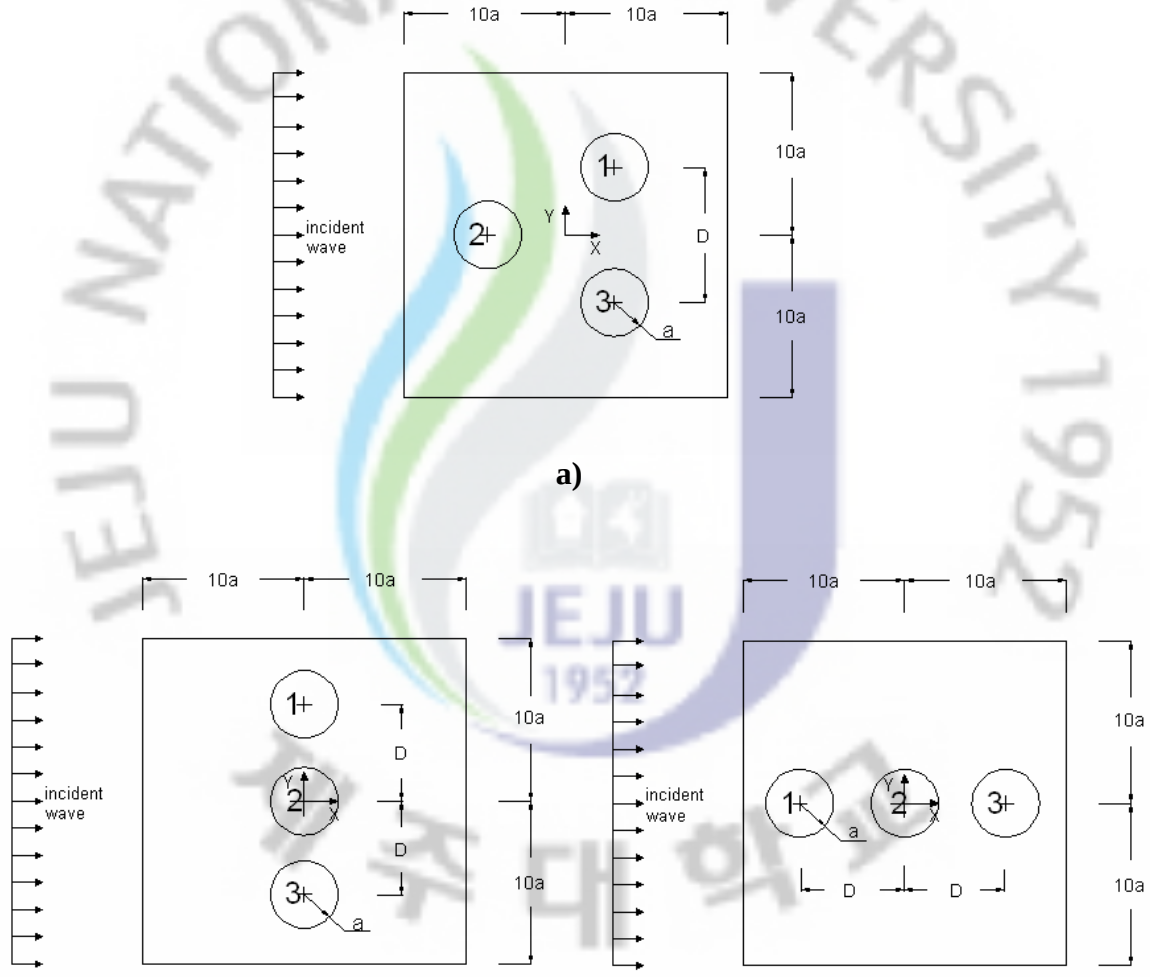

Fig. 28 Geometries for: (a) Three cylinders in triangular array, (b) Three cylinders in row array, (c) Three cylinders in column array

Fig. 29 and Fig. 30 show the wave forces in x-direction and y-direction acting on cylinder 1 and cylinder 2 in triangular array versus wave number ka. Due to the symmetry of the geometry, the wave forces in x-direction and y-direction on the cylinder 1 and cylinder 3 are the same and the wave forces in y-direction on cylinder 2 is zero.

Fig. 31 and Fig. 32 show the wave forces in x-direction and y-direction acting on cylinder 1 and cylinder 2 in row array versus wave number ka. In this geometry, the wave forces in x-direction and y-direction on the cylinder 1 and cylinder 3 are the same and the wave forces in y-direction on cylinder 2 is zero.

Fig. 33 shows the wave forces in x-direction acting on the cylinders in column array versus wave number ka. The wave forces in y-direction are zero.

The computed results show that due to the interaction of the cylinders, the graphs of wave forces acting on the cylinders in three different geometries are quite different with the wave forces acting on isolated cylinder. In triangular array and column array, the wave forces reach the maximum value near $ka = 0.5$. However in row array, the wave forces reach the maximum value near $ka = 0.3$. Also, the computed results are strong agreement with those of Ohkusu (1974).

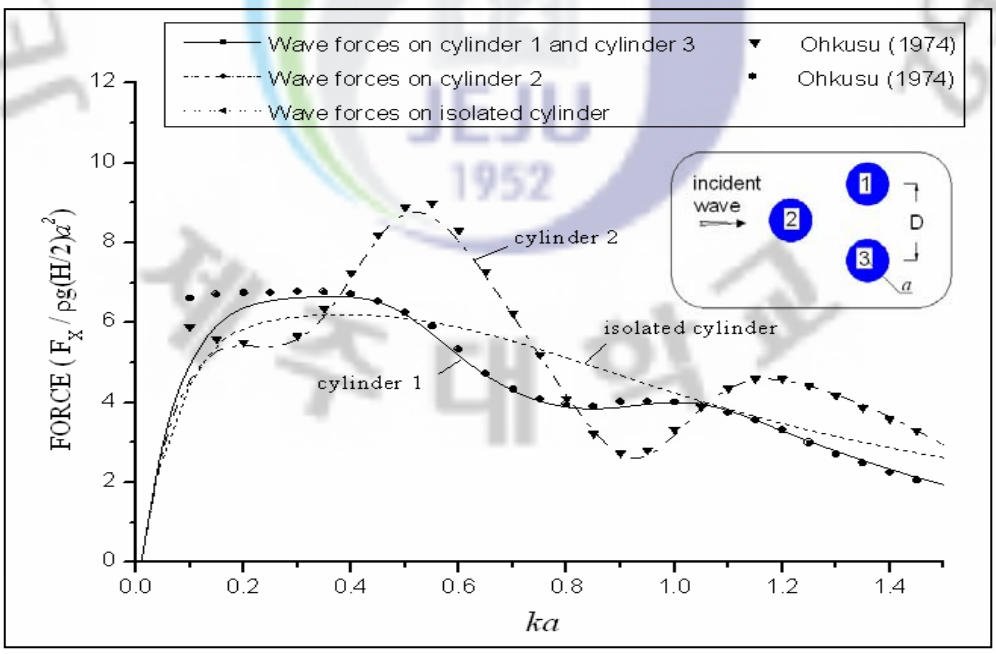

Fig. 29 Wave forces in x-direction acting on cylinder 1 and cylinder 2 in triangle array versus wave number ka for $h/a = 10,\ D/a = 5$

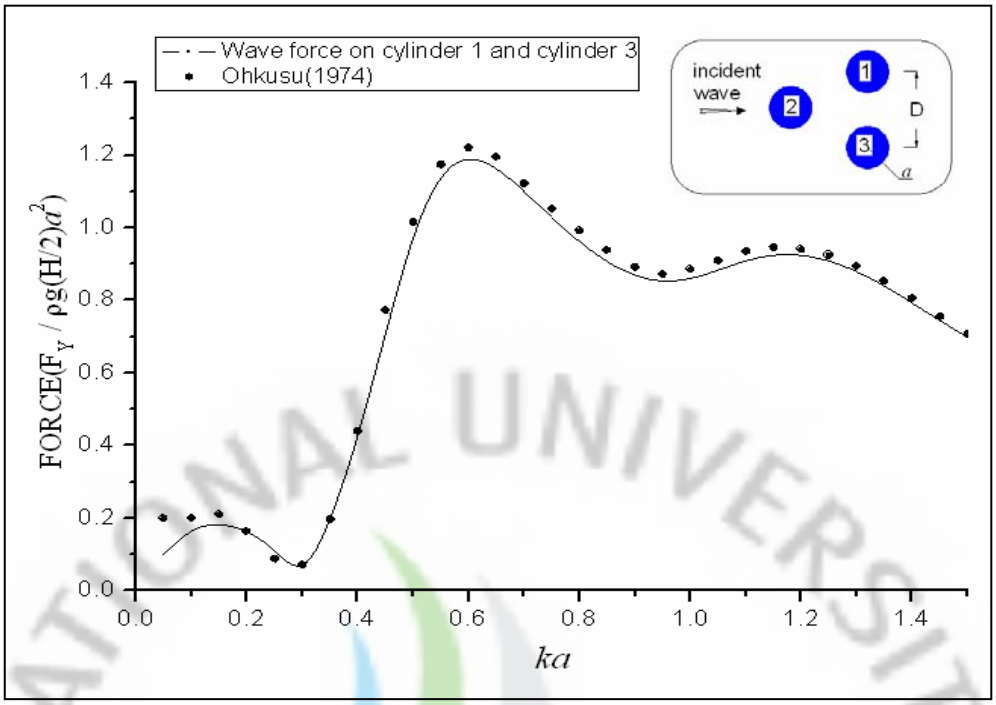

Fig. 30 Wave forces in y-direction acting on cylinder 1 and cylinder 3 in triangle array versus wave number ka for $h/a=10,\ D/a=5$

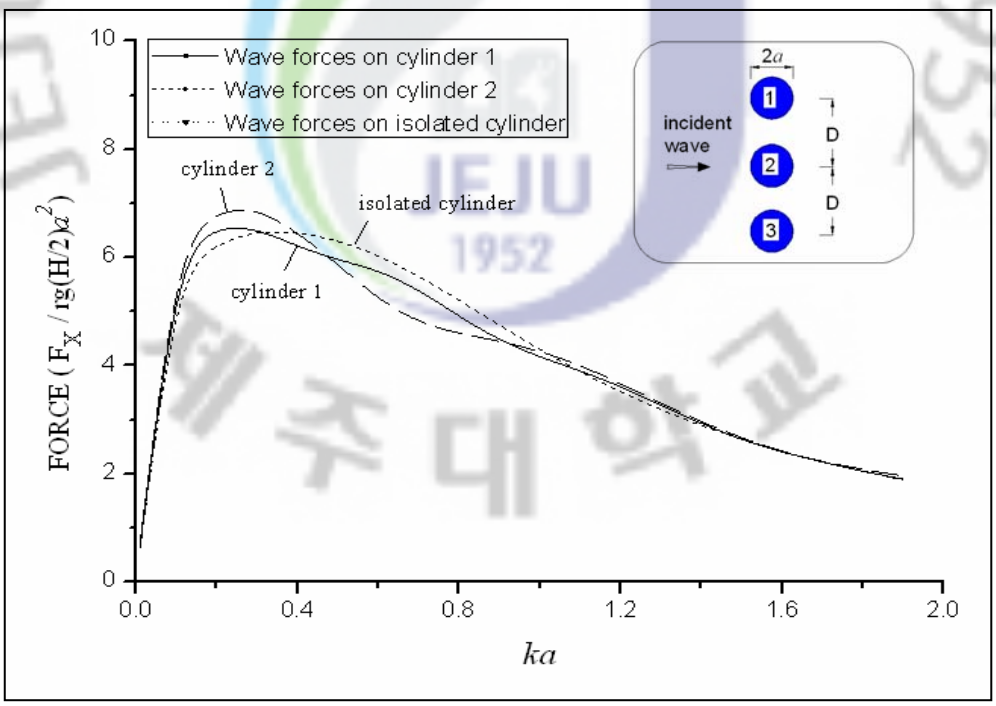

Fig. 31 Wave forces in x-direction acting on cylinder 1 and cylinder 2 in row array versus wave number ka for $h/a=10,\ D/a=5$

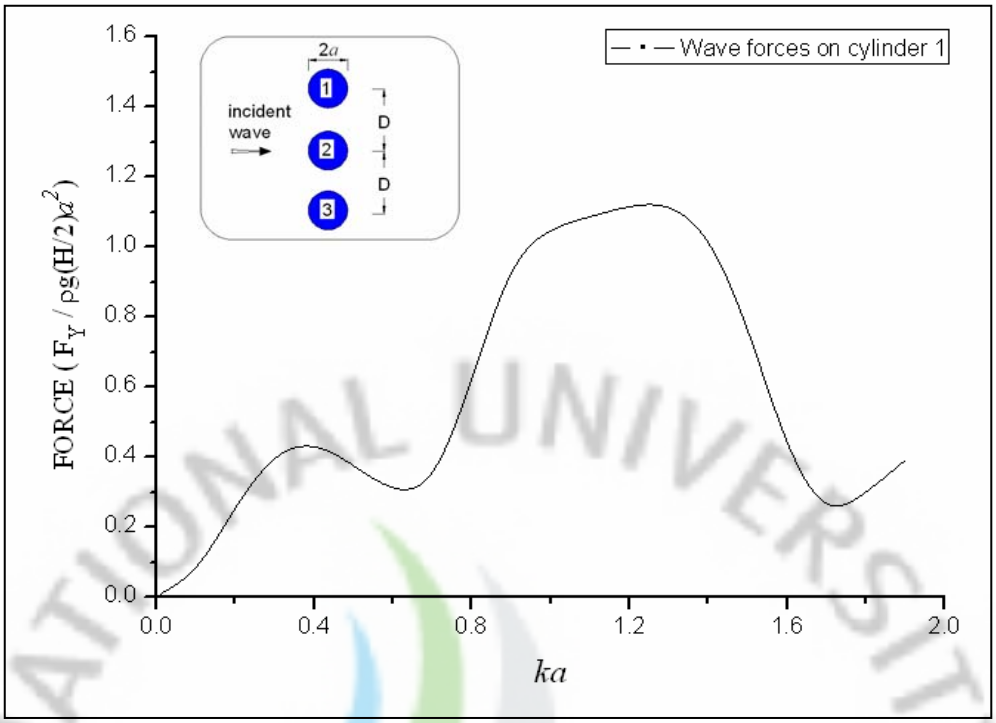

Fig. 32 Wave forces in y-direction acting on the cylinders in row array versus wave number ka for $h/a=10,\ D/a=5$

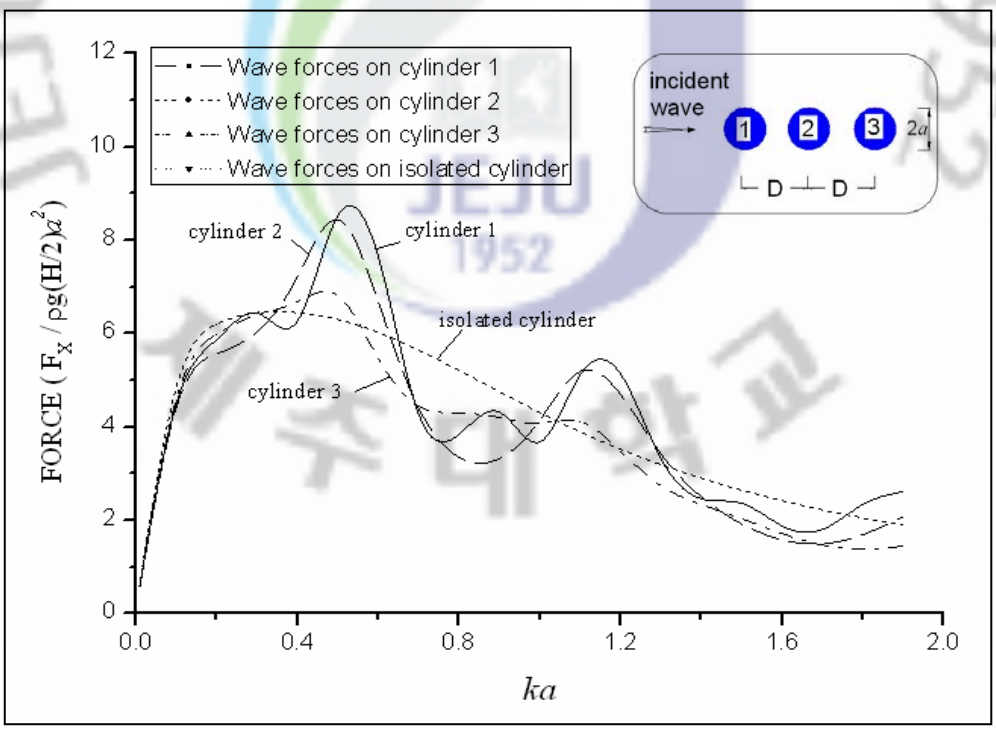

Fig. 33 Wave forces in x-direction acting on the cylinders in column array versus wave number ka for $h/a=10,\ D/a=5$

4.2.1 The Effects of Cylinder Spacing on Wave Forces on Three Vertical Circular Cylinders

The effects of the cylinder spacing on the wave forces acting on three cylinders are also investigated in this study. Fig. 34 to Fig. 36 show the wave forces in x-direction and y-direction acting on the cylinders in triangular array versus the ratio $\gamma = 2a/D$ for three special wave numbers $ka = 0.1, 0.5, 1.0$. In this geometry, the wave forces in x-direction and y-direction acting on cylinder 1 and cylinder 3 are the same, the wave forces in y-direction acting on cylinder 2 is zero.

The computed results show that the wave forces acting on three cylinders oscillate extremely large around the wave forces acting on an isolated cylinder as the ratio $\gamma \geq 0.2$.

Also, the computed results are strong agreement with those of Chakrabarti (1978).

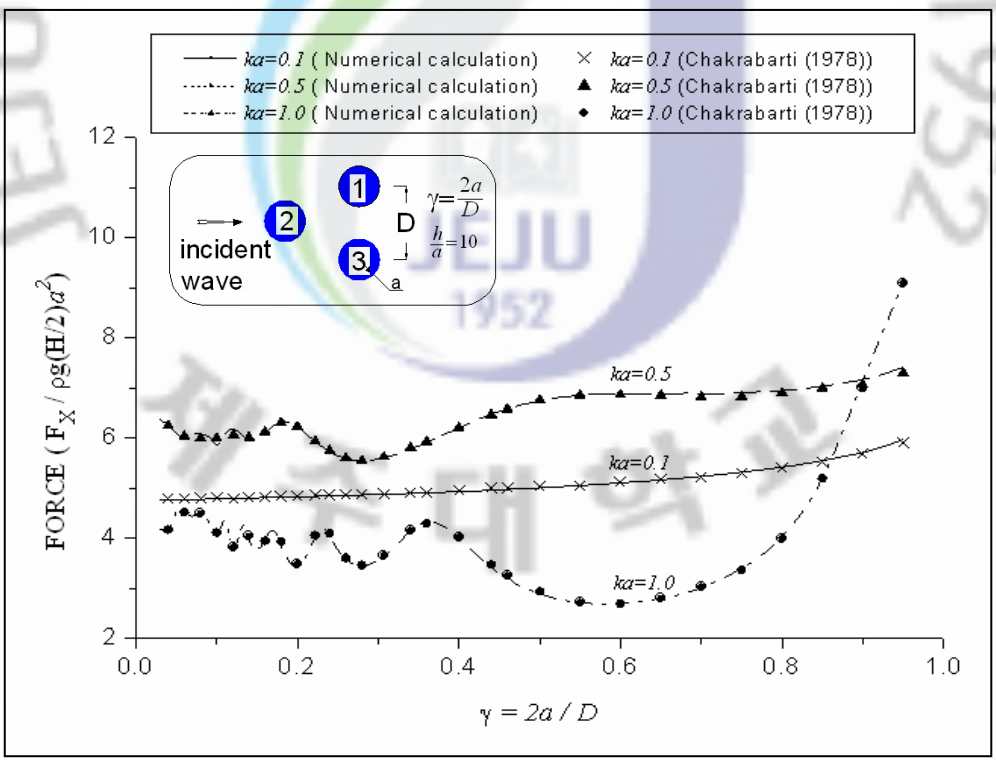

Fig. 34 Wave forces in x-direction acting on cylinder 1 in triangular array versus the ratio $\gamma = 2a/D$ for $h/a = 10$

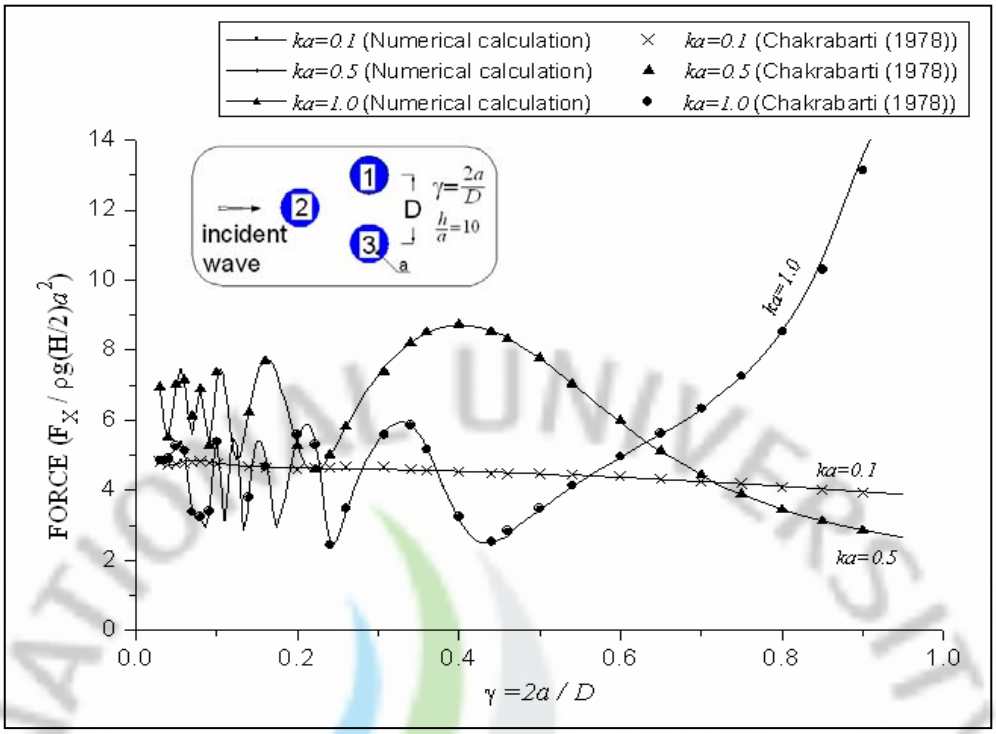

Fig. 35 Wave forces in x-direction acting on cylinder 2 in triangular array versus the ratio $\gamma = 2a/D$ for $h/a = 10$

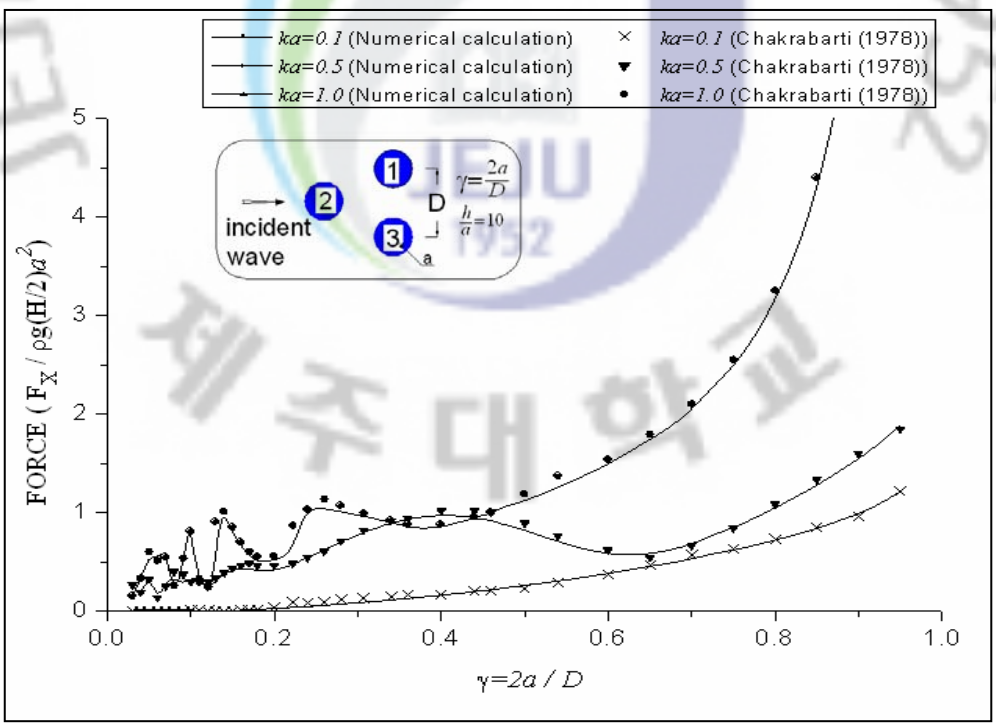

Fig. 36 Wave forces in y-direction acting on cylinder 1 in triangular array versus the ratio $\gamma = 2a/D$ for $h/a = 10$

Fig. 37 to Fig. 39 show the wave forces in x-direction and y-direction acting on three cylinders in row array versus the ratio $\gamma = 2a/D$ for three special wave numbers $ka = 0.1, 0.5, and\ 1.0$. The wave forces in x-direction and y-direction acting on cylinder 1 and cylinder 3 are the same, the wave forces in y-direction acting on cylinder 2 is zero.

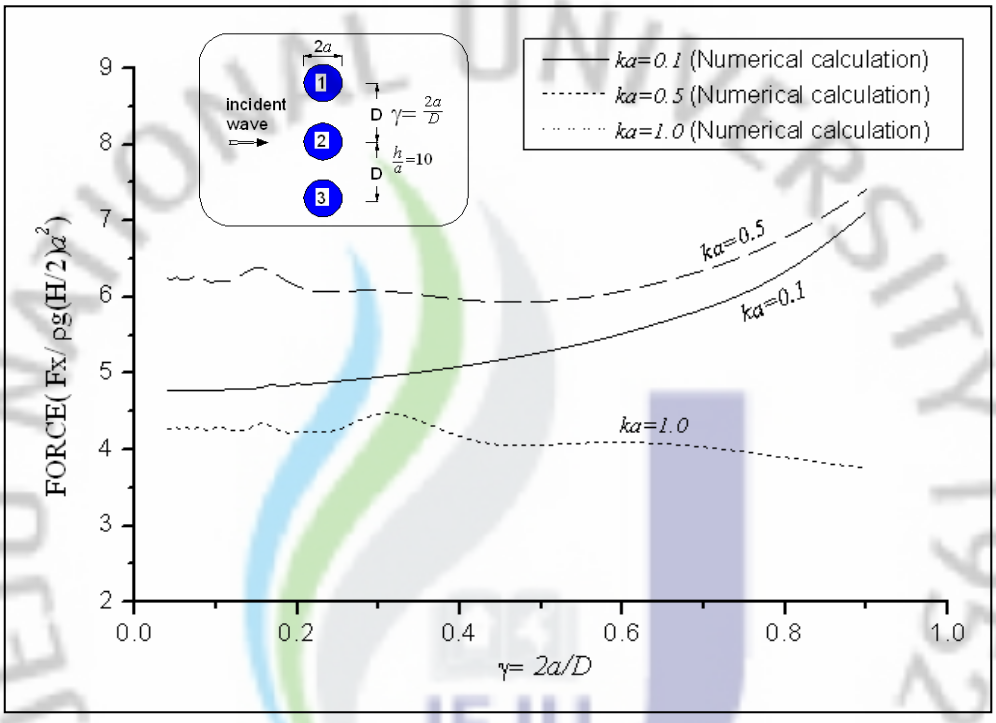

Fig. 37 Wave forces in x-direction acting on cylinder 1 in row array versus the ratio $\gamma = 2a/D$ for $h/a = 10$

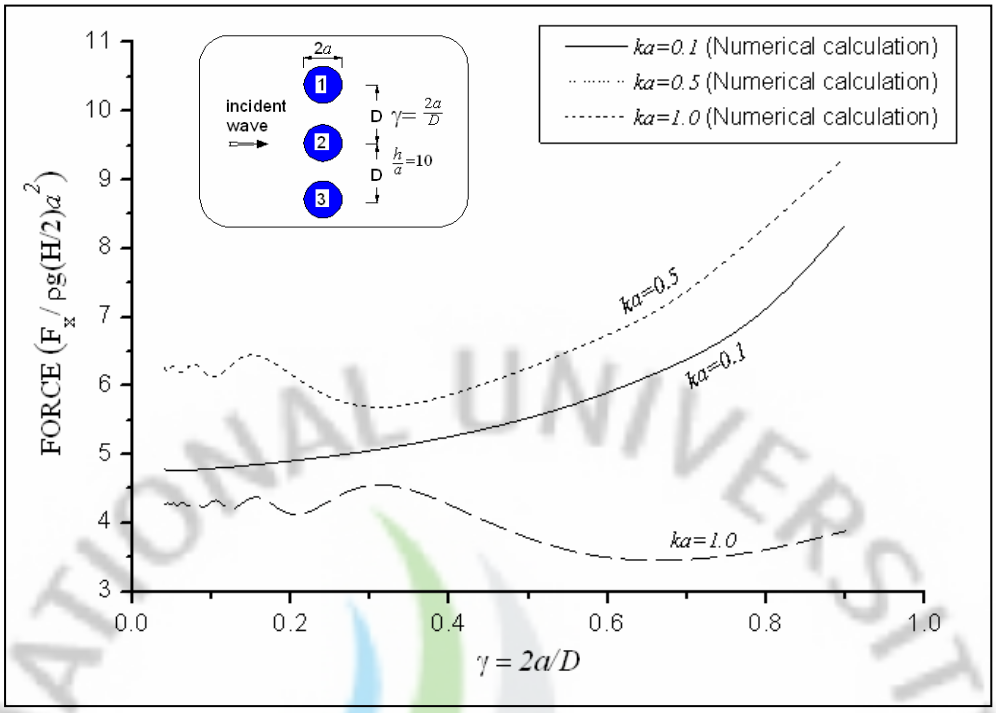

Fig. 38 Wave forces in x-direction acting on cylinder 2 in row array versus the ratio $\gamma = 2a/D$ for $h/a = 10$

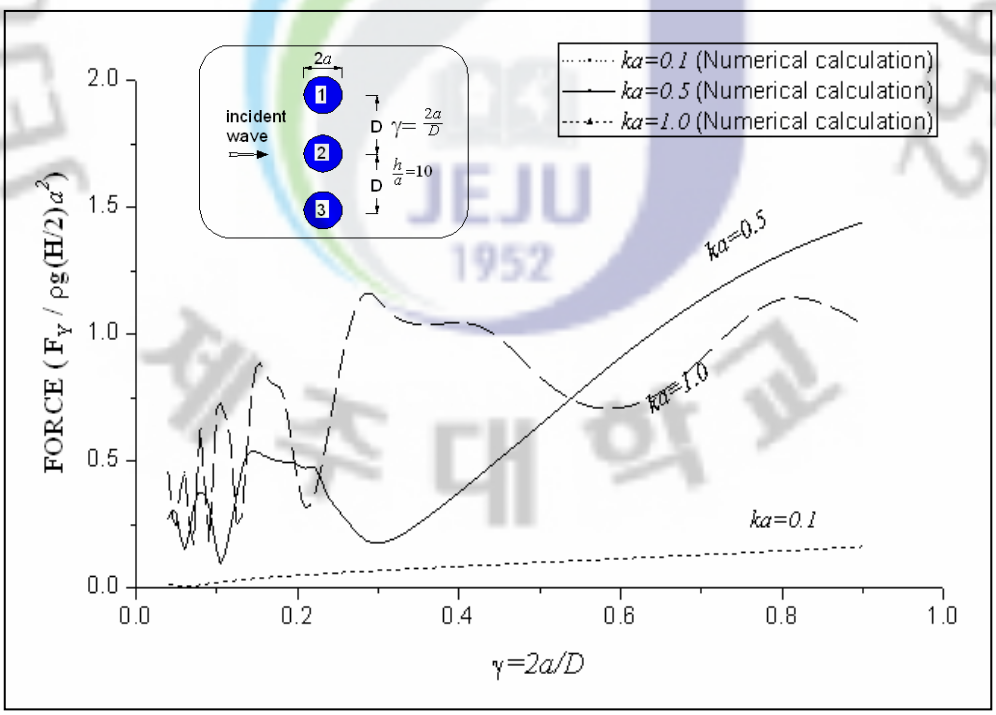

Fig. 39 Wave forces in y-direction acting on cylinder 1 in row array versus the ratio $\gamma = 2a/D$ for $h/a = 10$

Fig. 40 to Fig. 42 show the wave forces in x-direction acting on three cylinders in column array versus the ratio $\gamma = 2a/D$ for three special wave numbers $ka = 0.1, 0.5, \text{and } 1.0$. Due to the symmetry of this geometry, the wave forces in y-direction are zero.

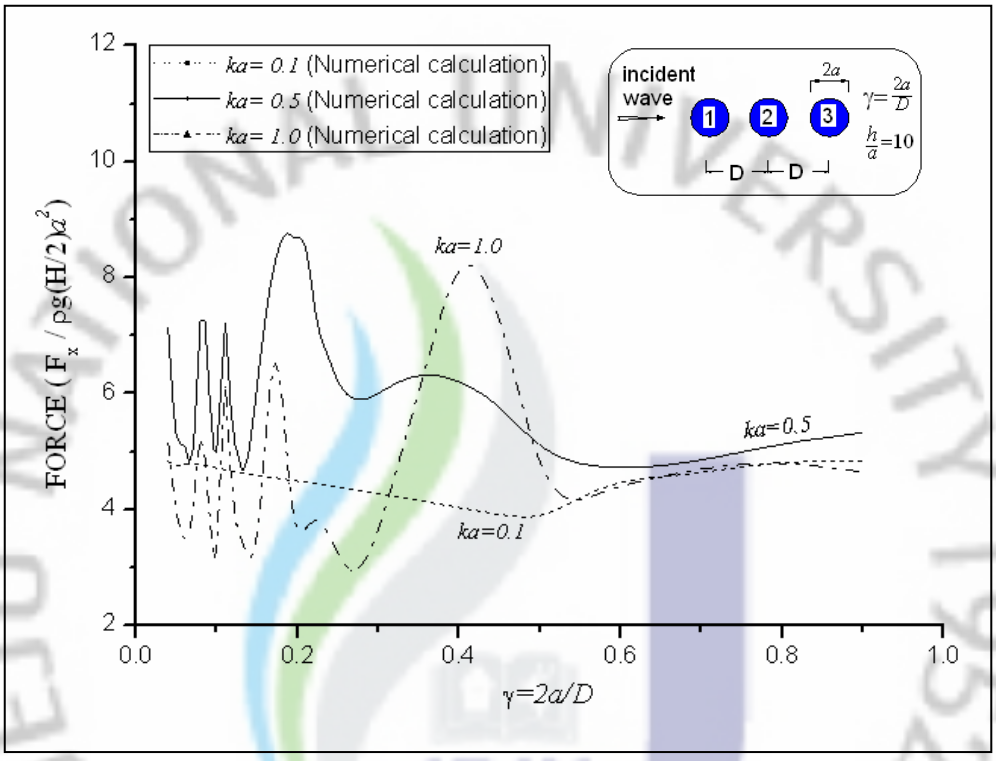

Fig. 40 Wave forces in x-direction acting on cylinder 1 in column array versus the ratio $\gamma = 2a/D$ for $h/a = 10$

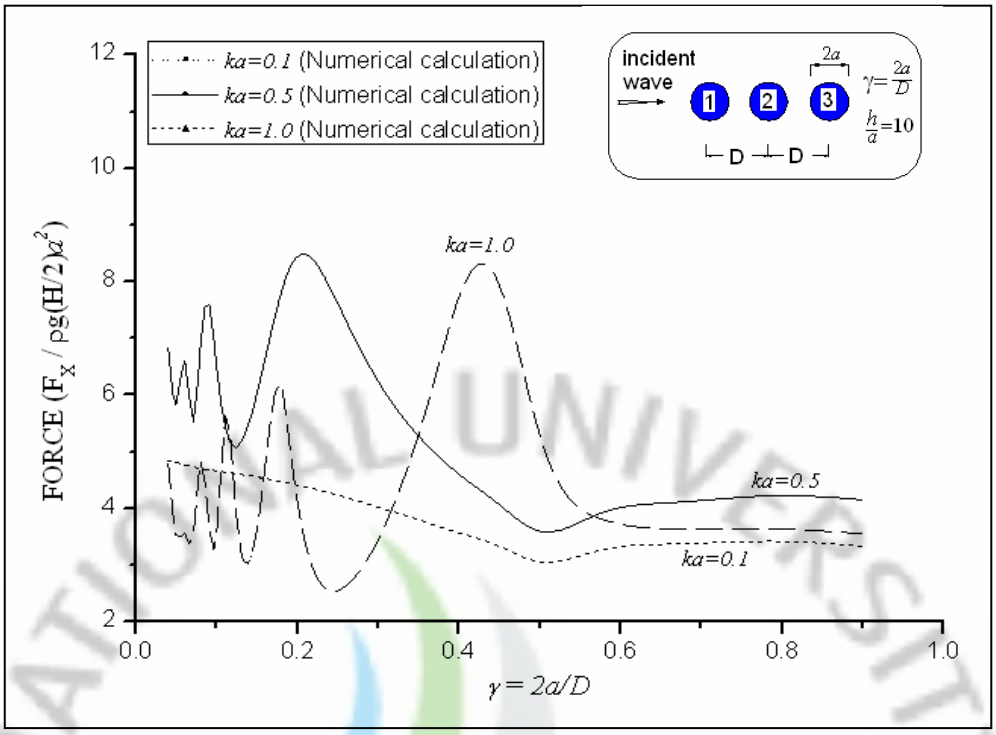

Fig. 41 Wave forces in x-direction acting on cylinder 2 in column array versus the ratio $\gamma = 2a/D$ for $h/a = 10$

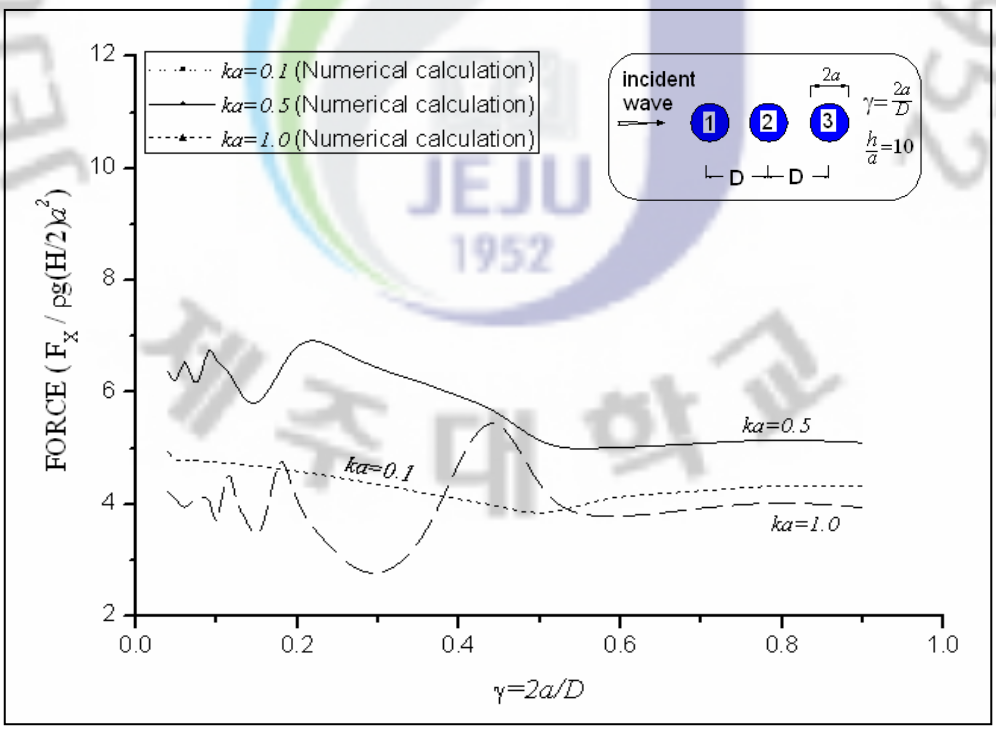

Fig. 42 Wave forces in x-direction acting on cylinder 3 in column array versus the ratio $\gamma = 2a/D$ for $h/a = 10$

4.2.2 The Effects of Incident Wave Angle on Wave Forces on Three Vertical Circular Cylinders

The effects of incident wave angle on the wave forces acting on three cylinders are studied in this paper. Fig. 43 to Fig. 51 show the wave forces acting on three cylinders in three different geometries as the incident waves are propagating at various angles $\beta = 0^0, 30^0, 45^0, 60^0$. The numerical results show that the wave forces acting on the cylinders in x-direction tend to decrease gradually as the incident wave angle increases.

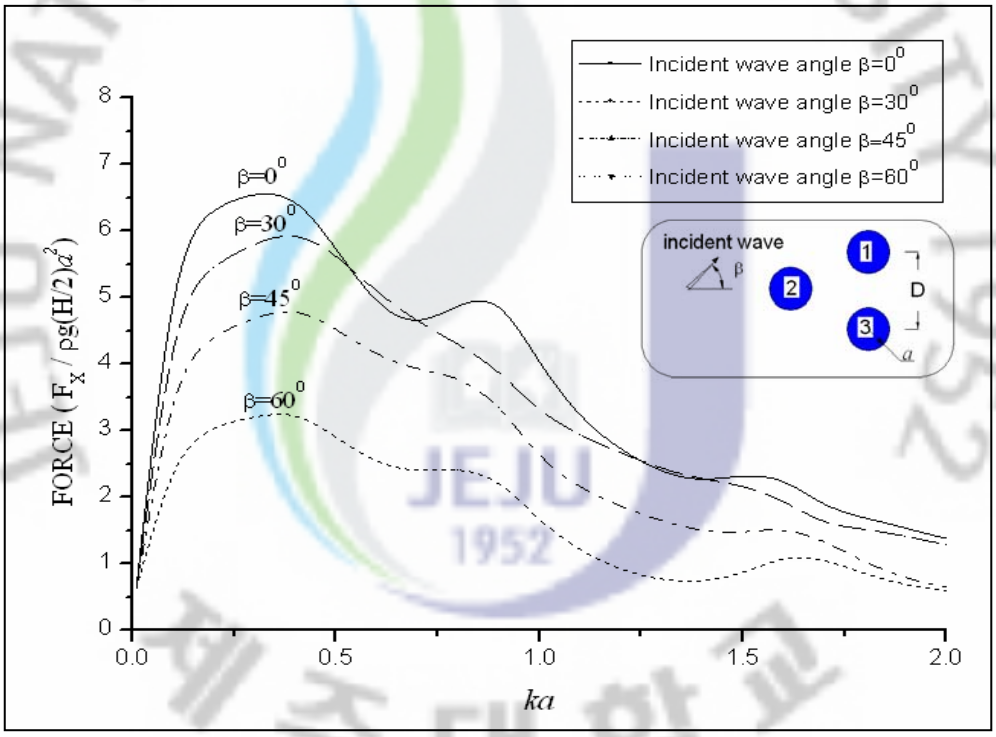

Fig. 43 Wave forces in x-direction acting on cylinder 1 in triangular array with four different incident wave angles $\beta = 0^0, 30^0, 45^0, 60^0$ for $h/a = 10, D/a = 6$

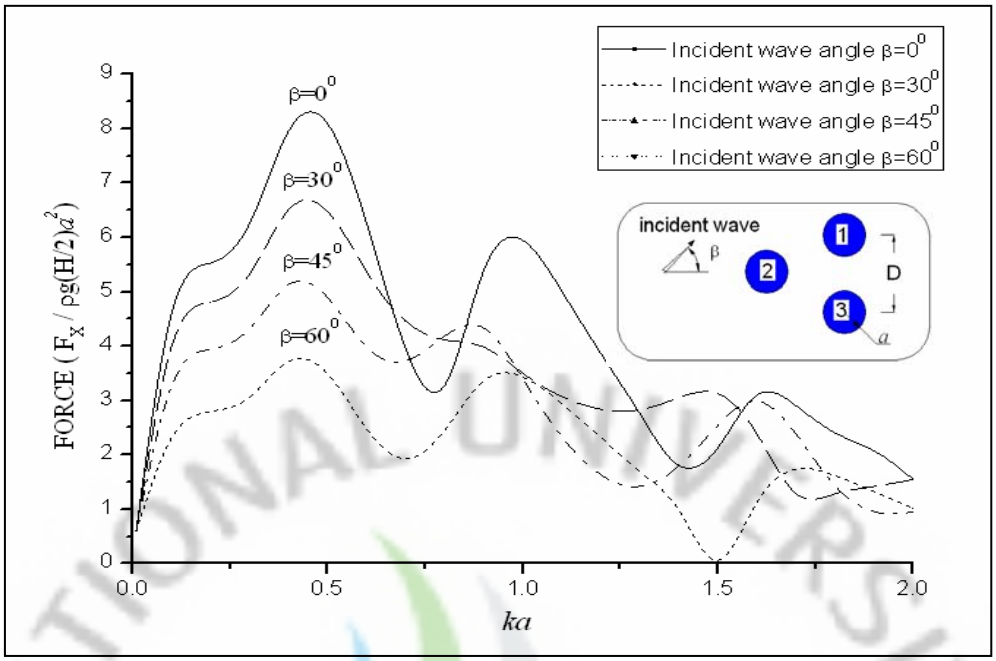

Fig. 44 Wave forces in x-direction acting on cylinder 2 in triangular array with four different incident wave angles $\beta = 0^0, 30^0, 45^0, 60^0$ for $h/a = 10, D/a = 6$

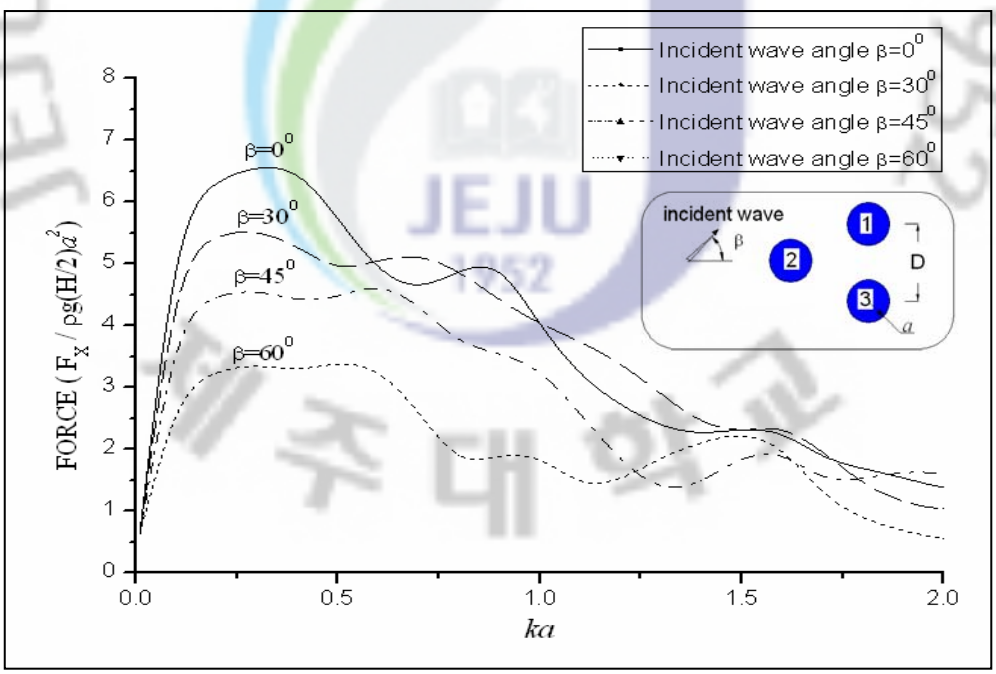

Fig. 45 Wave forces in x-direction acting on cylinder 3 in triangular array with four different incident wave angles $\beta = 0^0, 30^0, 45^0, 60^0$ for $h/a = 10, D/a = 6$

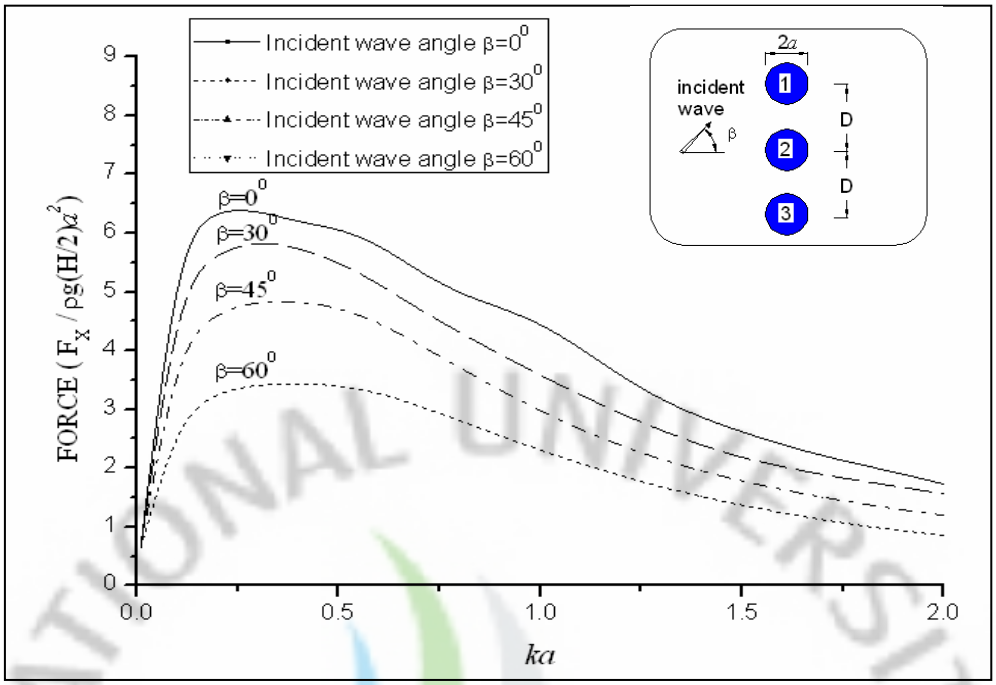

Fig. 46 Wave forces in x-direction acting on cylinder 1 in row array with four different incident wave angles $\beta = 0^0, 30^0, 45^0, 60^0$ for $h/a = 10, D/a = 6$

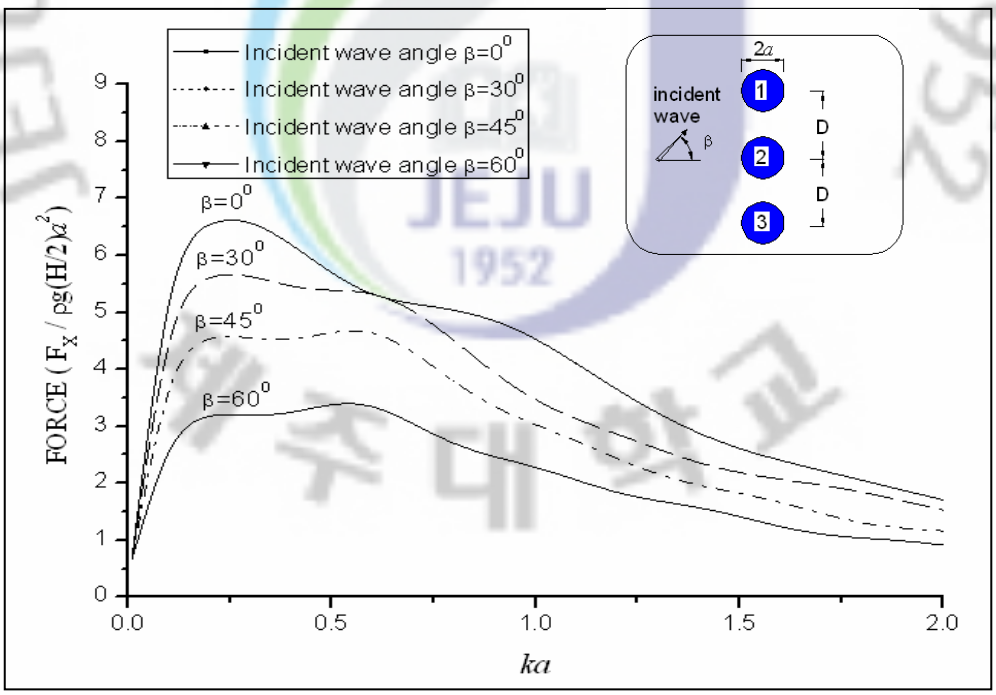

Fig. 47 Wave forces in x-direction acting on cylinder 2 in row array with four different incident wave angles $\beta = 0^0, 30^0, 45^0, 60^0$ for $h/a = 10, D/a = 6$

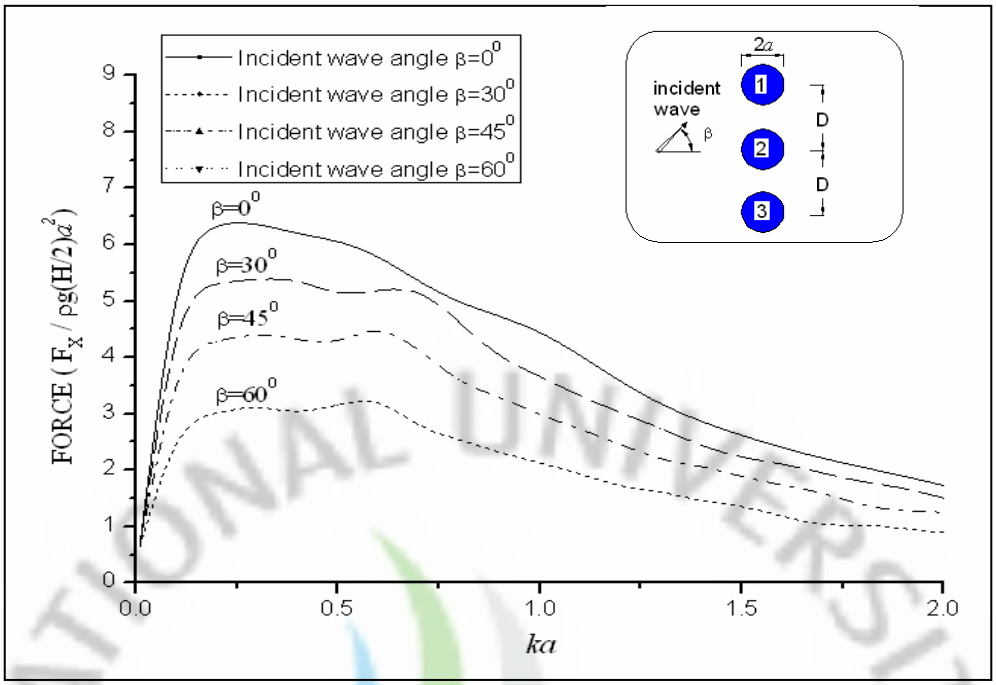

Fig. 48 Wave forces in x-direction acting on cylinder 3 in row array with four different incident wave angles $\beta = 0^0, 30^0, 45^0, 60^0$ for $h/a = 10, D/a = 6$

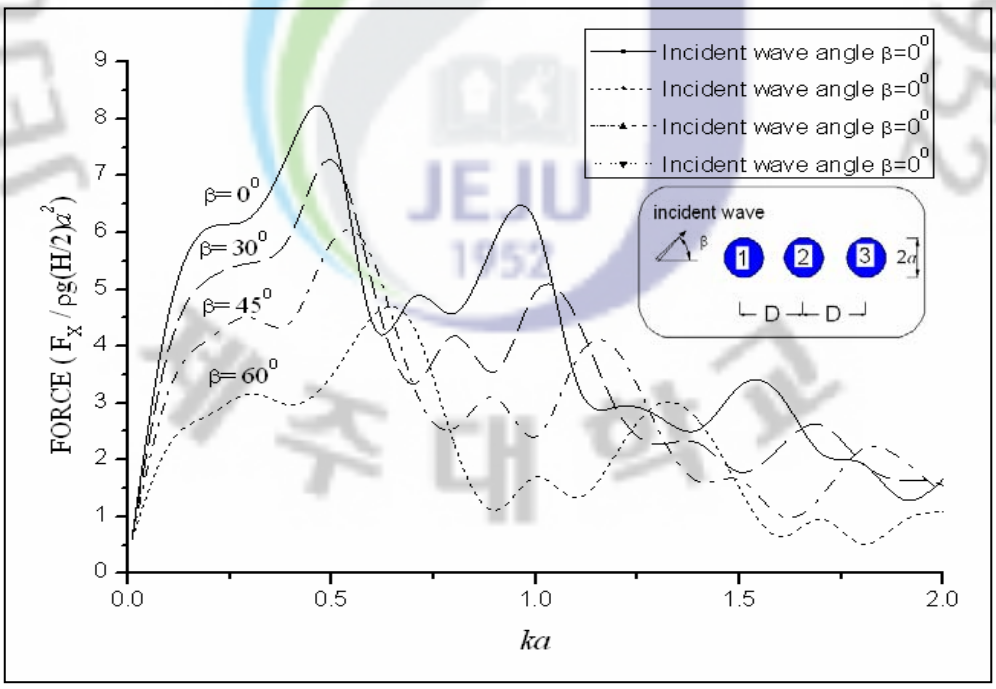

Fig. 49 Wave forces in x-direction acting on cylinder 1 in column array with four different incident wave angles $\beta = 0^0, 30^0, 45^0, 60^0$ for $h/a = 10, D/a = 6$

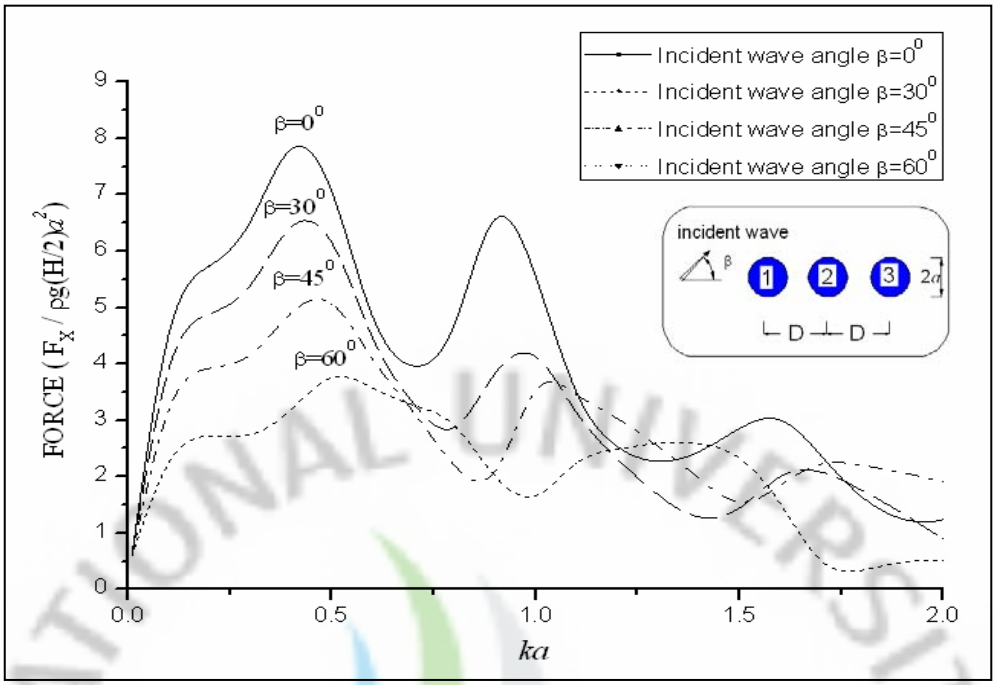

Fig. 50 Wave forces in x-direction acting on cylinder 2 in column array with four different incident wave angles $\beta = 0^0, 30^0, 45^0, 60^0$ for $h/a = 10, D/a = 6$

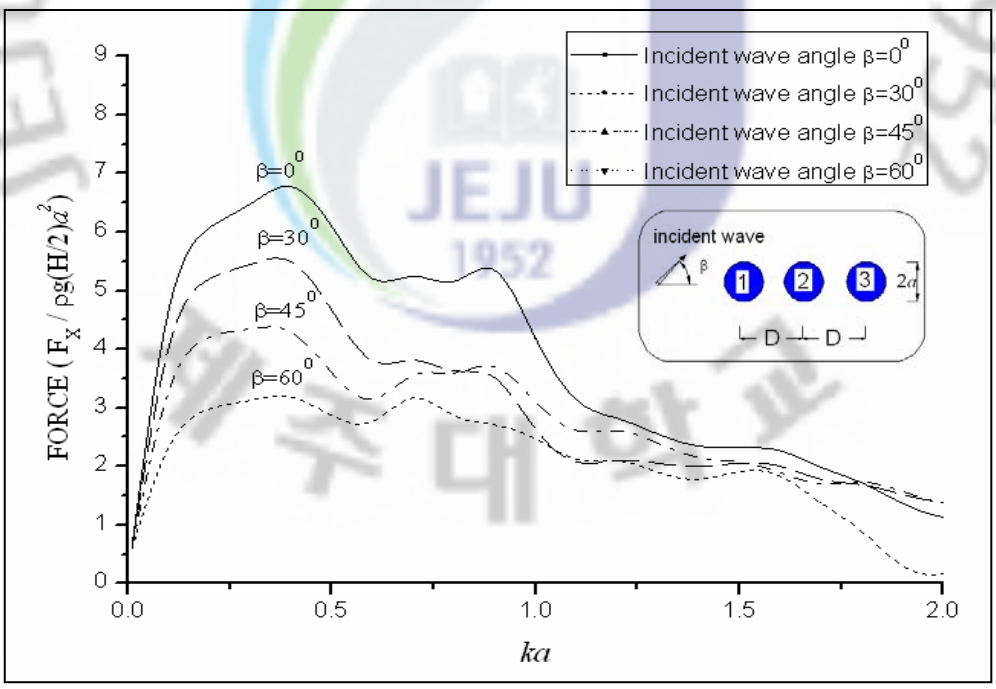

Fig. 51 Wave forces in x-direction acting on cylinder 3 in column array with four different incident wave angles $\beta = 0^0, 30^0, 45^0, 60^0$ for $h/a = 10, D/a = 6$

4.2.3 Run-up on the Outer Walls of Three Vertical Circular Cylinders

Fig. 52 to Fig. 54 shows the computed results of run-up on the outer walls of three cylinders in triangular array, row array and column array for special wave number $ka = 1.0$. The magnitude of run-up is nondimensionalized by wave height *H*. The results show that the run-up profiles of the cylinders are quite different from that of an isolated cylinder due to the interaction of the cylinders. In addition to, the run-up profiles are quite different with different geometries.

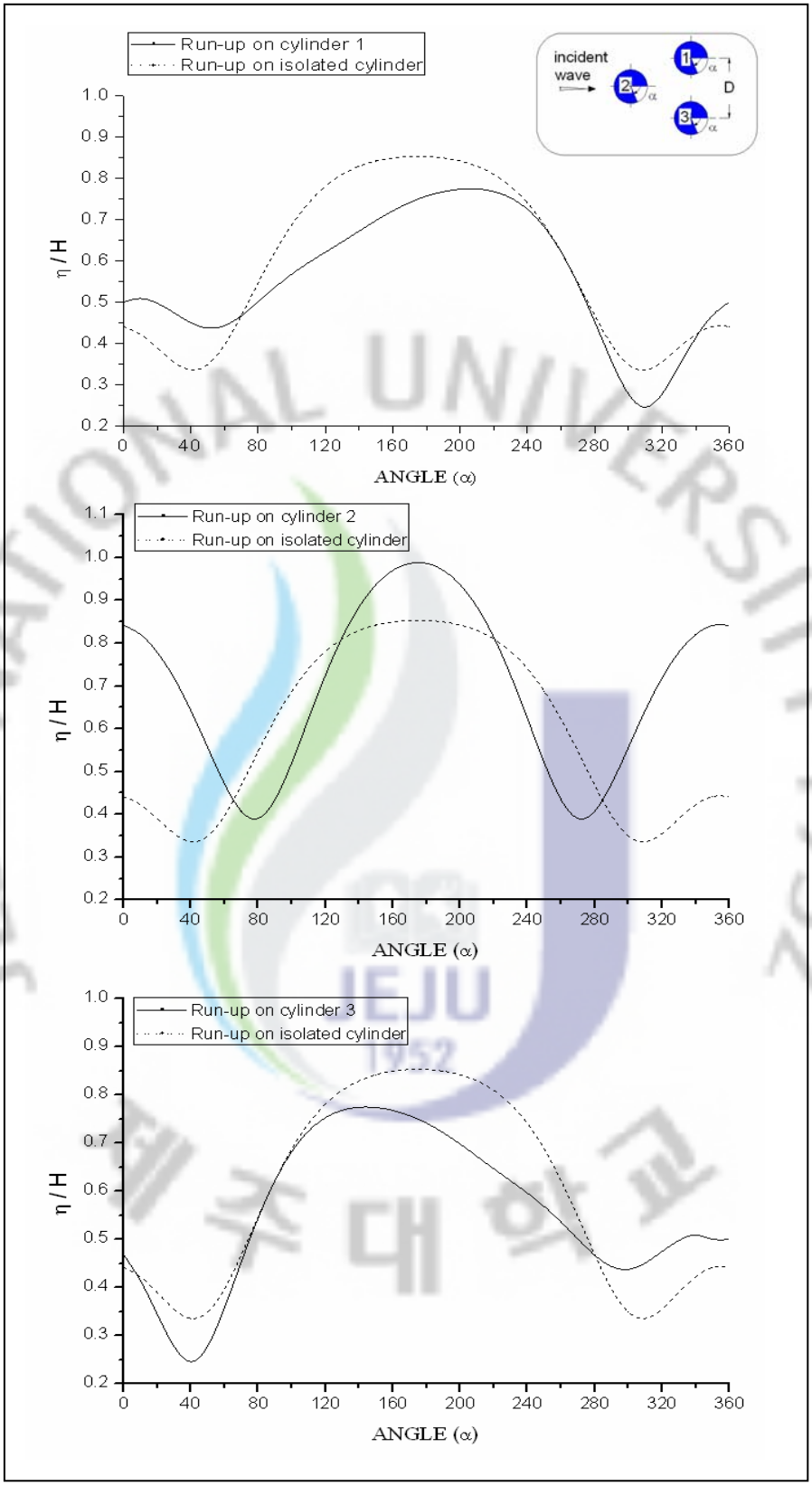

Fig. 52 Run-up on the outer walls of three cylinders in triangular array for $h/a = 10, D/a = 6, ka = 1.0$

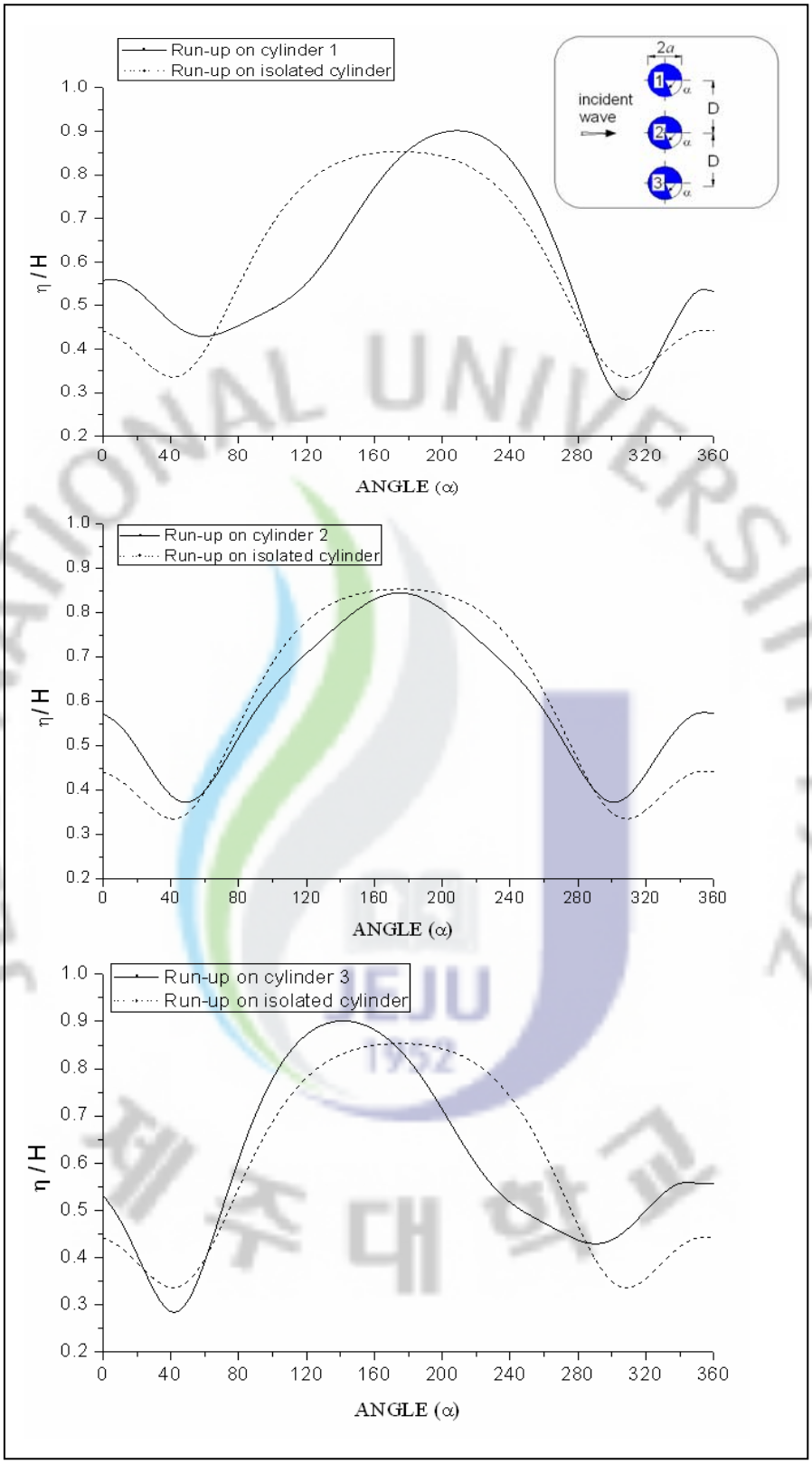

Fig. 53 Run-up on the outer walls of three cylinders in row array for $h/a = 10, D/a = 6, ka = 1.0$

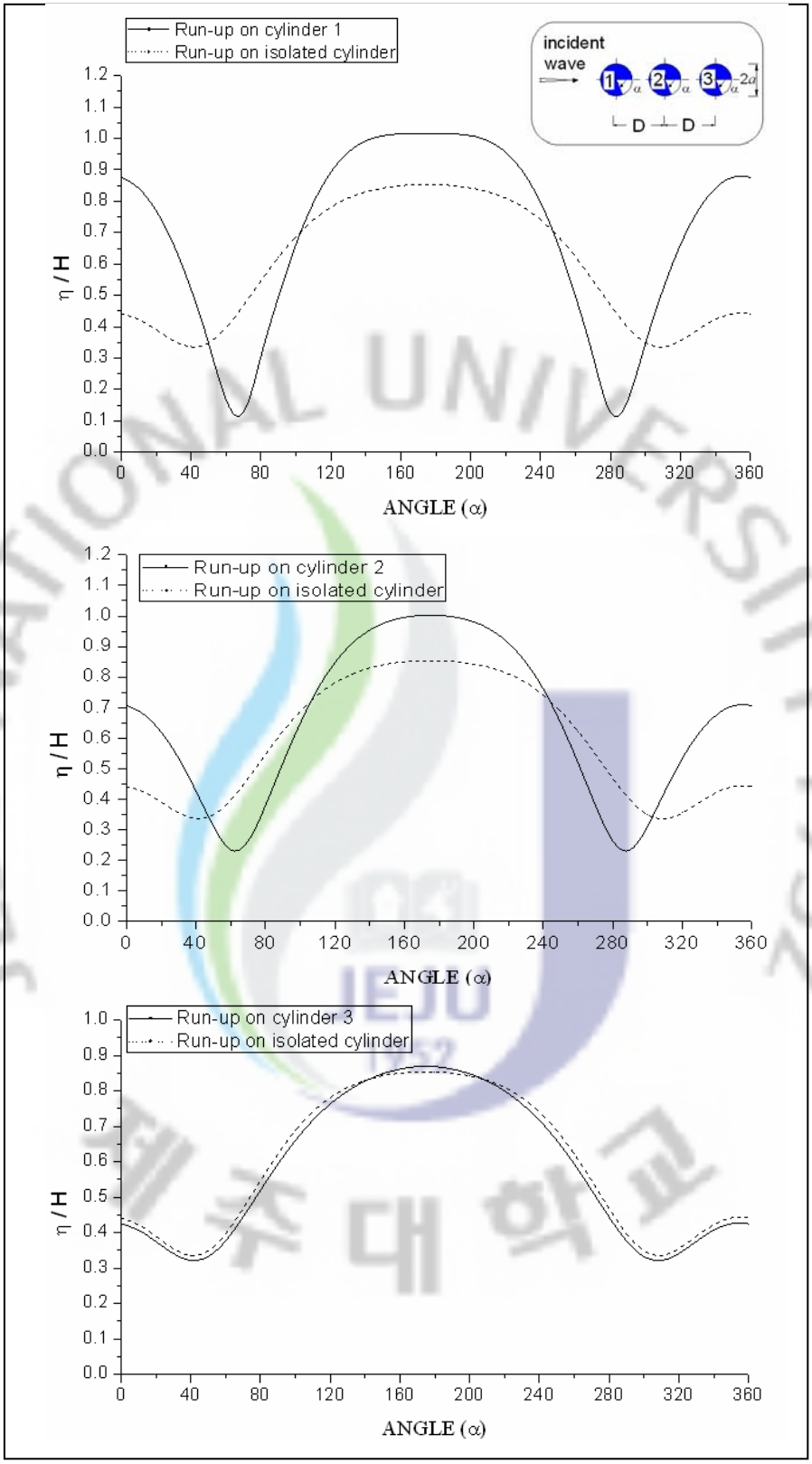

Fig. 54 Run-up on the outer walls of three cylinders in column array for $h/a = 10, D/a = 6, ka = 1.0$

4.2.4 Free-Surface Elevation around Three Vertical Circular Cylinders

Fig. 55 to Fig. 60 show the computed results of free-surface elevation contour and wave height distribution around three cylinders in three different geometries for special wave number $ka = 1.0$. The computed results present the same value as the run-up in Fig. 52 to Fig. 54.

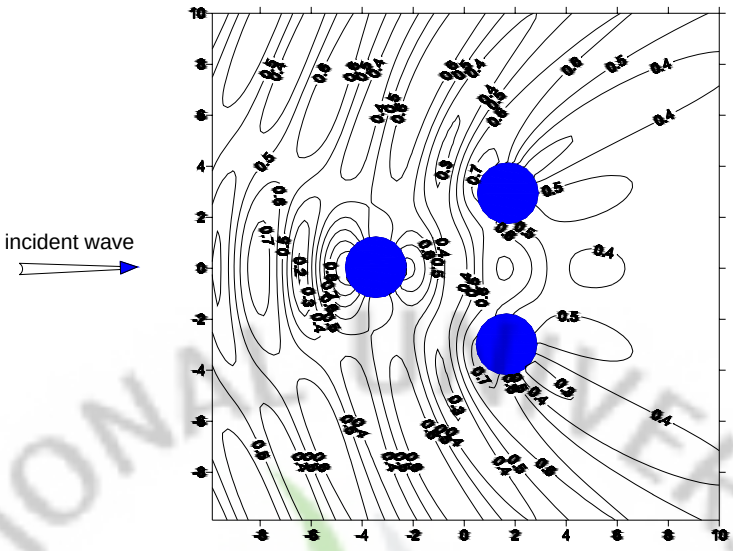

Fig. 55 Free-surface elevation contour around three cylinders in triangular array for $h/a=10, D/a=6, ka=1.0$

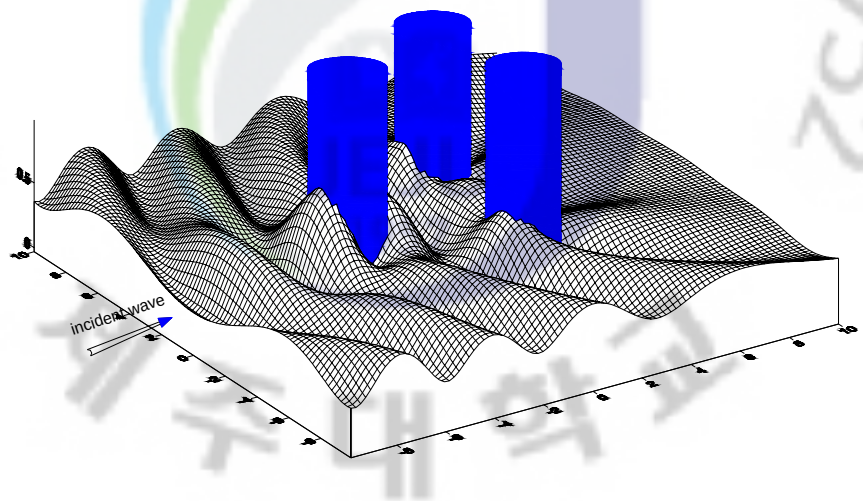

Fig. 56 Wave height distribution around three cylinders in triangular array using three-dimensional graphic technique for $h/a=10, D/a=6, ka=1.0$

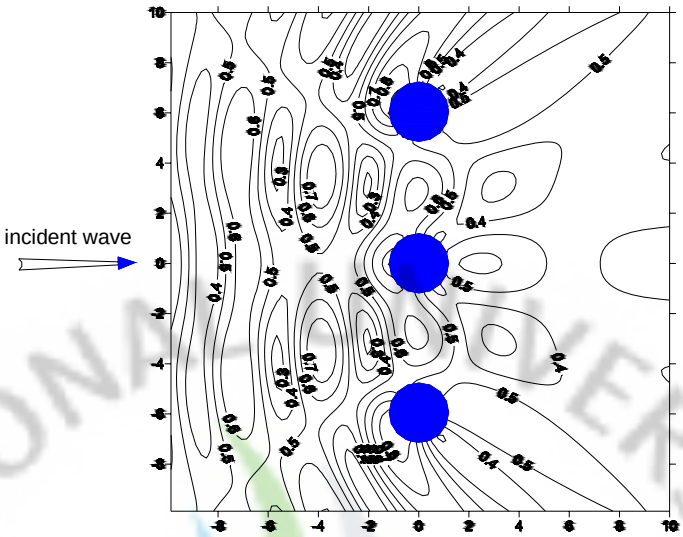

Fig. 57 Free-surface elevation contour around three cylinders in row array for $h/a = 10, D/a = 6, ka = 1.0$

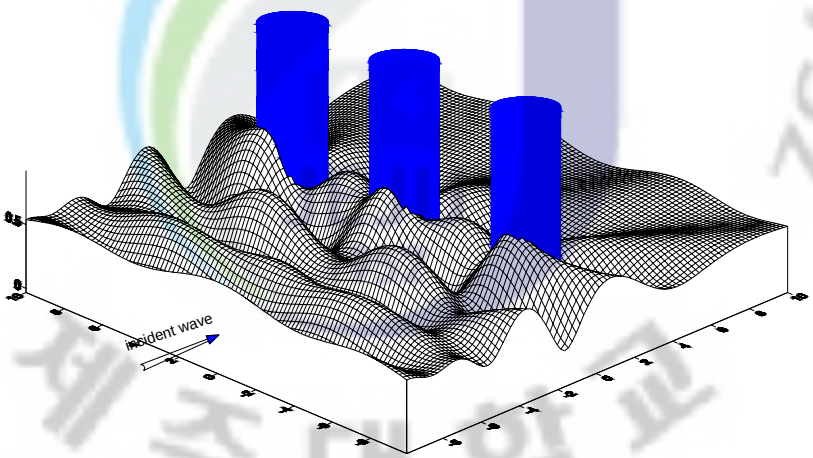

Fig. 58 Wave height distribution around three cylinders in row array using three-dimensional graphic technique for $h/a = 10, D/a = 6, \ ka = 1.0$

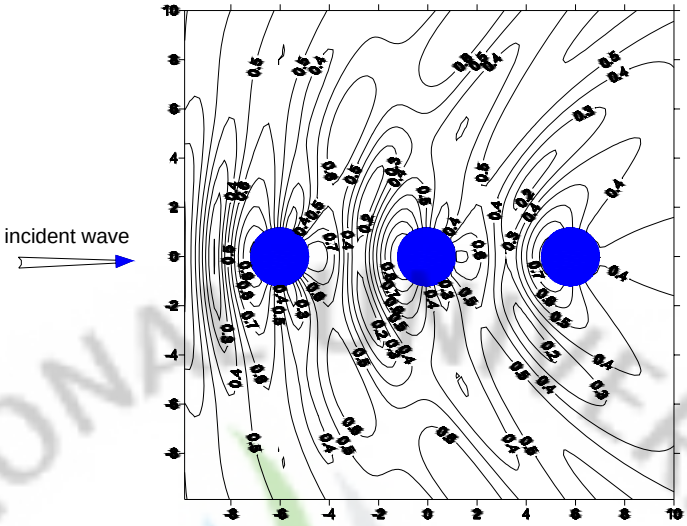

Fig. 59 Free-surface elevation contour around three cylinders in column array for $h/a=10, D/a=6, ka=1.0$

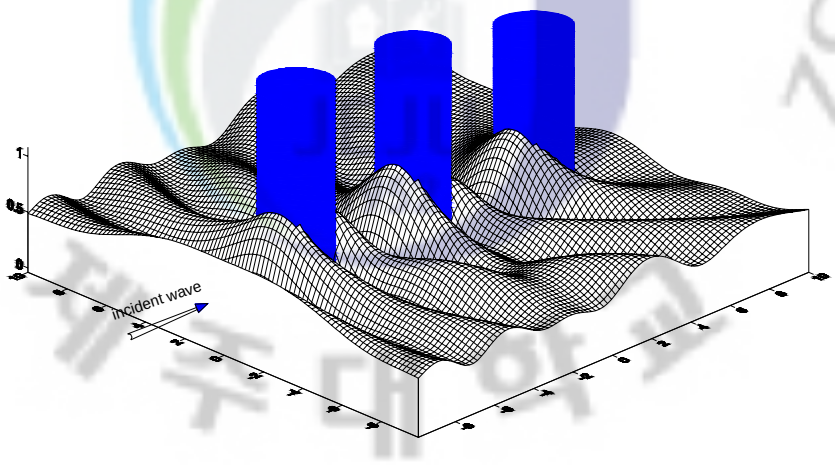

Fig. 60 Wave height distribution around three cylinders in column array using three-dimensional graphic technique for $h/a=10, D/a=6, ka=1.0$

Chapter 5
CONCLUSIONS AND REMARKS

A numerical analysis for the wave forces acting on multiple vertical circular cylinders has been derived. The wave forces acting on the cylinders are calculated by boundary element method using velocity potential ϕ. To verify this numerical method and to investigate the effects of the neighboring cylinders on the wave forces on a vertical cylinder, two-cylinder configuration and three-cylinder configuration are used in this study. The results obtained from this study are compared with those of Chakrabarti (1978) and Ohkusu (1974). The comparisons show the excellent agreement between the results of this study and their results. Thus, this numerical analysis by using boundary element method is verified.

Also in this study, several numerical examples are given in order to illustrate the effects of various parameters on the wave forces on the cylinders such as the cylinder spacing, the wave number and the incident wave angle. The run-up on the outer walls of the cylinders and wave height distribution around the cylinders are also calculated. The major results gained from this study are as follows:

(1) The maximum wave forces on the cylinders in two-cylinder configuration and three-cylinder configuration are higher than that on isolate cylinder due to the interaction of the cylinders.

(2) As the wave number increases, the wave forces acting on the cylinders oscillated around the wave forces acting on an isolated cylinder and the amplitude of oscillation of the wave forces on the front cylinder is larger than that on the back cylinder. The wave forces on the rear cylinder are reduced by the shielding effect.

(3) In two tandem cylinders, the wave forces on the cylinders reach maximum values near $ka = 0.5$.

(4) In three-cylinder configuration, the wave forces acting on three cylinders in triangular array and column array reach the maximum value near $ka = 0.5$. However in row array, the wave forces reach the maximum value near $ka = 0.3$.

(5) As the cylinder spacing increases, the wave forces acting on the cylinders in two-cylinder configuration and three-cylinder configuration do not decrease linear to the wave forces acting on an isolated cylinder, however it oscillates around the wave force amplitude on an isolated cylinder. The amplitude of oscillation is extremely large as the ratio $\gamma \geq 0.2$. As the cylinder spacing approaches infinity, the wave forces acting on the cylinders reach the wave force amplitude acting on an isolated cylinder.

(6) When incident wave is propagating at various angles $\beta = 0^0, 30^0, 45^0, 60^0$, the wave forces on the cylinders tend to decrease gradually as the incident wave angle increases.

(7) Due to the interaction among the cylinders, the run-up profiles of the cylinders in two-cylinder configuration and three-cylinder configuration are quite different from that of an isolated cylinder. The run-up on the front cylinder is higher than that on the back cylinder because the shielding effect.

This numerical analysis will be used broadly in the design of vertical cylinders to be constructed in the coastal zones in the future.

References

김남형 · 서일교 공역. 1995. 경계요소법기초. 원창출판사.
김남형 · 박구용 · 조일형 공역. 2004. 해안파동. 구미서관.

Chakrabarti, S.K. (1978), Wave forces on multiple vertical cylinders, Journal of Waterway, Port, Coastal and Ocean Division, Vol. 104, No. 2, pp. 147-161.

Chakrabarti, S.K. (2000), Hydrodynamic interaction forces on multi-moduled structures, Ocean Engineering, Vol. 27, No. 10, pp. 1037-1063.

Han, K.M. and Ohkusu, M. (1995), Wave forces on groups of vertical circular cylinders, Research Papers, Ocean Resources Research Institute Dong-A University, Vol. 8, No. 1, pp. 17-26.

Honji, H. 1981, Streaked flow around an oscillating cylinder, J. of Fluid Mech., Vol. 107, pp. 509-520.

Isaacson, M. 1978, Vertical cylinder of arbitrary section in waves. Journal of waterway, Port, Coastal and Ocean division, ASCE 104(WW4), pp.309-324.

Isaacson, M. 1979, Wave-induced forces in the diffraction regime. In: Mechanics of Wave-Induced Forces on Cylinders, (Ed. T.L Shaw). Pitman Advances Publishing Program, pp. 68-69.

John, F. 1950, On the motion of floating bodies II. Comm. Pure & Appl. Math., Vol. 3, No. 1, pp. 45-101.

Justesen, P. (1989): Hydrodynamic forces on large cylinders in oscillatory flow. J. Waterway, Port, Coastal and Ocean Engineering, ASCE, 115(4):497-514.

Kagemoto, H. and Yue, D.K.P. (1986), Interaction among multiple three-dimensional bodies in water waves, Journal of Fluid Mech., Vol. 166, pp. 189-209.

Kim, M.H. (1992), Interaction of waves with N vertical circular cylinders, Journal of Waterway, Port, Coastal, and Ocean Engineering, ASCE, Vol. 119, No. 6, pp. 671-689.

Kim, N.H. and Cao, T.N.T. (2008), Wave force analysis of the two vertical cylinders by boundary element method. KSCE Journal of Civil Engineering, Vol.12, No.6, pp.359-366.

Kim, N.H. and Cao, T.N.T. (2008), Wave force analysis of the three vertical cylinders in water waves. International Journal of Navigation and Port Research, Vol.32, No.7, pp.543-552.

Kim, N.H. and Park, M.S. (2007), Wave force analysis of the vertical circular cylinder by boundary element method, KSCE Journal of Civil Engineering, Vol. 11, No. 1, pp. 31-35.

Linton, C.M., Evans, D.V. (1990), The interaction of waves with arrays of vertical circular cylinders. J. Fluid Mech. No. 46, pp. 549-569.

MacCamy, R.C. and Fuchs, R.A. (1954) Wave forces on piles: a diffraction theory, Tech. Memo, No.69, US Army corps of Engineering, Beach Erosion Board.

Ohkusu, M. (1974), Hydrodynamic forces on multiple cylinders in waves, In Proc. Intl Symp. on Dynamics of Marine Vehicles and Structures in Waves, London, Paper 12, pp. 107-112.

Sarpkaya, T. (1976a): In-line and transverse forces on smooth and sand-roughened cylinders in oscillatory flow at high Reynolds numbers. Naval Postgraduate School, Monterey, CA, Tech. Rep. NPS-69SL76062.

Sarpkaya, T. (1986a): Force on a circular cylinder in viscous oscillatory flow at low Keulegaan-Carpenter numbers. J. Fluid Mech., 165:61-71.

Spring, B.H. and Monkmeyer, P.L.(1974), Interaction of plane waves with vertical cylinders, Proceedings of the fourteenth international conference on coastal engineering, Copenhagen, Denmark, ASCE, pp. 1828-1847.

Twersky, V. (1950), Multiple scattering of radiation by an arbitrary configuration of parallel cylinders, Journal of the Acoustical Society of America, Vol. 24, pp 42-46.

Williams, A.N. and W. Li. (2000), Water wave interaction with an array of bottom-mounted surface-piercing porous cylinder, Ocean Engineering, Vol. 27, No. 8, pp. 841-866.

Williamson, C.H.K. (1985): Sinusoidal flow relative to circular cylinders. J. Fluid Mech., Vol. 155, pp. 141-174.

Xianchu, Z., Dongjiao, W., and Chwang, A.T. (1997), Hydrodynamic interaction between two vertical cylinders in water waves, English Edition, Vol. 18, No. 10.

ACKNOWLEDGEMENT

First of all I wish to thank God for his continuous help and support.

This thesis work was done at the Department of Civil and Ocean Engineering, Graduate School of Engineering, Cheju National University, Korea. This thesis would not have been possible without the supports and assistances of professors, colleagues, and my family, to whom I would like to express my gratitude.

I am deeply indebted to my supervisor Professor Nam-Hyeong Kim for providing good guidance to this research throughout my study in Cheju National University. Especially, I am grateful for his moral and economical support which enabled me to concentrate on my research and to write this thesis. His experiences and vast knowledge in the field were great important to this thesis. I will always keep in mind his various teachings during my study.

I would like to express my sincere gratitude to Professor Sang-Jin Kim and Professor Byoung-Gul Lee, for their invaluable suggestions and discussions on the research topic. I also would like to thank Professor Seong-Gi Yang, Jung-Man Nam, Dong-Wook Lee and Sang-Yeol Park for giving me invaluable advices, helping me and giving me helpful comments when I faced problems during my study in Cheju National University.

I would like to express my sincere gratitude to Pastor Choi, Byung Ha and all of people in the Immanuel Methodist Church for their invaluable moral and financial supports. As a foreign student, I faced with many problems such as homesick, financial problems, and culture shocks. However, Pastor Choi brought me to the God and I received a warm relationship with all people in the Immanuel Methodist Church.

I also want to thank all members of Coastal and Harbor Engineering Laboratory, Cheju National University: Mr. Haeng-Sik, Mr. Kang-Il, Mr. Min-Su, Miss Hyang-He, Miss Ji-Won, Hyeong-Chul, Sung-Hwan, U-Suk, Seung-Hyun, Chang-Lim, Hyun-Chul,

Su-Min, Ju-Kyung and all of my seniors, the same classes, juniors in Coastal and Harbor Engineering Laboratory and Civil and Ocean College for their warm friendship, helping , and encouragements. As a foreign student, I received a lot of help and advices in studying and living in Korea from them.

Lastly, I wish to express my thanks to my family for their continuous support and encouragement during my study in Korea. I am most thankful to my wife, Nguyen Thi Ngoc Lan, who has been separated for years during my research in Korea. Thank you a lot for bearing a lot of difficulties during my research.

February, 2009

Cao Tan Ngoc Than

List of Papers

◆ Refereed Journal Paper

①. “Wave Force Analysis of the Two Vertical Cylinders by Boundary Element Method.” KSCE Journal of Civil Engineering, Vol.12, No.6, pp.359-366, 2008 (in Korea)

②. “Wave Force Analysis of the Three Vertical Cylinders in Water Waves.” International Journal of Navigation and Port Research, Vol.32, No.7, pp.543-552, 2008 (in Korea)

◆ Proceedings of Annual Conference

③. “Wave Force Analysis Acting on Two Vertical Cylinders by Boundary Element Method.” *Proceeding of the Korean Annual Conference on Civil Engineering*, pp. 3655-3656, 2007 (in Korea)

④. “ Wave Force Analysis of the Three Vertical Cylinders in Water Waves, *Proceeding of the Korean Annual Conference on Marine Engineering*, pp. 309-310, 2008 (in Korea)

⑤. “Wave Force Analysis of the Four Vertical Cylinders in Water Waves.” *Proceeding of the Korean Annual Conference on Civil Engineering*, pp. 4259-4262, 2008 (in Korea)